Transient Liquid-phase Infiltration of Aluminum Alloys

by

Vinay Kumar Prabhakar

Bachelor of Technology (Hons.), Mechanical Engineering
Indian Institute of Technology, Kharagpur, 1999

Submitted to the Department of Mechanical Engineering
in partial fulfillment of the Requirements for the degree of

MASTERS OF SCIENCE IN MECHANICAL ENGINEERING

at the

MASSACHUSETTS INSTITUTE OF TECHNOLOGY

SEPTEMBER 2002

Signature of author: .....
Department of Mechanical Engineering
August 16, 2002

Certified by: .....
Emanuel M. Sachs
Fred Fort Flowers and Daniel Flowers Professor of Mechanical Engineering
Thesis Supervisor

Accepted by: .....
Prof. Ain A. Sonin
Chairman, Graduate Committee

Transient Liquid-phase Infiltration of Aluminum Alloys

by

Vinay Kumar Prabhakar

Submitted to the Department of Mechanical Engineering on August 16, 2002
In partial fulfillment of the requirements for the Degree of
Masters of Science in Mechanical Engineering

ABSTRACT

The ability to fabricate direct aluminum metal parts using Solid Freeform Fabrication (SFF) processes would create tremendous opportunities because of their combination of high strength, corrosion resistance, and high thermal and electrical conductivity. This has been achieved by combination of 3D Printing, a SFF process, and Transient Liquid-phase Infiltration (TLI) technique. Green parts of desired shape and complexity can be directly made from a CAD model by 3D Printing process using pure aluminum powder. It is then densified near full density using TLI, which is a capillary induced infiltration process that uses an infiltrant similar to the powder material, but containing a melting point depressant, usually some common alloying element. This thesis is focused on later.

Densification of aluminum powder metal parts by infiltration is very difficult because of presence of thick, dense natural oxide skin on the surface of both infiltrant melt and powder skeleton, which prevents wetting. The problem is even worse in the case of SFF processes where there is no mechanical breakage of oxide layer, which generally occurs during mechanical compaction in conventional powder metallurgy processes. This necessitates a controlled furnace atmosphere with better control of oxygen content in the work zone for processing of the parts. A gettering system has been designed using aluminum as getter charge, which removes oxygen from the gas inflow before entering the work zone and ensures cleaner furnace atmosphere. A dipping mechanism has been developed using ceramic foam filter, which mechanically break the thick oxide layer present on the surface of the infiltrant melt, and filters out clean liquid melt for infiltration. The problem of wetting was solved using a wetting agent, magnesium, in the infiltrant melt. It enhances wetting by chemically breaking the oxide skin on the powder surface. Magnesium being more reactive than aluminum preferentially reacts with oxygen and reduces aluminum oxide breaking its skin from the powder surface. Successful infiltration of 1" tall sample has been achieved with infiltrant containing 11-13 % Si and 2-4 % Mg. Microstructure study, compositional analysis and mechanical testing were done to characterize the infiltrated parts. Infiltrated parts with density up to 95% of theoretical density have been achieved. The infiltrated parts have hardness comparable to similar aluminum alloys

Thesis Supervisor: Emanuel M. Sachs

Title: Fred Fort Flowers and Daniel Flowers Professor of Mechanical Engineering

Acknowledgements

I would like to express my sincere gratitude to my advisor, Prof. Emanuel Sachs, for giving me an opportunity to work on this project and providing me with constant support, guidance, and encouragement. I have learnt a lot while working with him and truly enjoyed interacting with him over the last two years. I am thoroughly impressed by his ability to come up with simple solutions to seemingly complex problems.

Next, I would like to thank Prof. Samuel Allen, for his insightful guidance in the field of metallurgy and materials science research.

I would also like to thank the following people who helped me during my research work:

Adam Lorenz, for providing me a great insight of TLI and being a good colleague, ever ready to use his knowledge to assist me solve problems.

Calvin Yuen, for helping me in SEM analysis and materials research.

Jim Serdy, for helping me in every possible way with his great expertise and experience with 3DP and making things go a little easier in the lab.

Brian, for giving me great ideas for the processing of aluminum from his extensive experience with this material system and making me familiar me with all the issues.

Julie, Heather, Liev, and Laura, for promptly processing my order requests and helping me in all non-technical and administrative stuff.

Mark and Gerry, for making all my visits to machine shop a nice experience and assisting me in operating different machines and part fabrications.

Yin-Lin Xie of Materials Science, for helping me in doing metallography of my specimens.

Thanks to Blake, Lucas, Nathan, Ae, Chris, David, Diana, Jermy, Nate, and others who made my stay in the 3D printing lab a memorable one. Also, thanks to all my friends for making my stay at both MIT and outside it a truly enjoyable experience.

Special thanks to the Office of Naval Research (Dr. Ralph Wachter) and Extrude Hone Corporation (NIST ATP) for funding the research work.

Finally, I would like to thank my parents and sisters for all their love and encouragement, without which this work would not have been possible.

Table of Contents

List of Figures

List of Tables

Chapter 1. Introduction

1.1 Three Dimensional Printing

Three Dimensional printing (3DP) is a solid freeform fabrication (SFF) process for rapid and flexible production of prototype parts, end-use parts, and tools directly from a CAD model [2]. It builds parts layer by layer by joining powdered material with a binder. The process starts with a CAD model of the desired part. The part model is sliced into thin layers using a slicing algorithm, which draws detailed information for every layer. Each layer begins by spreading a thin layer of powder over the surface of the powder bed. A computer-controlled printhead derives information for each layer from the computer model and prints binder over the powder bed like ink-jet printing, selectively joining powder particles where the object is to be formed. The powder bed is then lowered, another powder layer is spread, and binder is deposited to print the next cross-section. This process is repeated until the whole part is generated. Figure 1.1 shows the steps involved in 3DP.

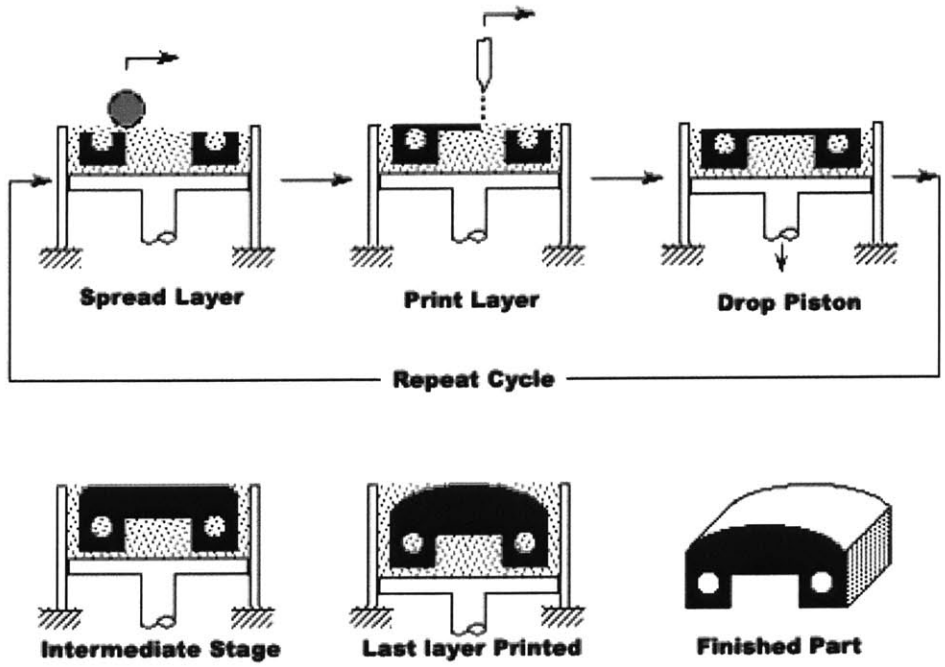

Figure 1.1 3DP process cycle

Three dimensional printing process has unprecedented flexibility and can create parts of any shape, geometry, and out of any material, including ceramics, metals, polymers, and composites. Furthermore, it can exercise local control over the material composition, microstructure, and surface texture making it a very useful process for many applications.

1.2 Direct Metal Parts

3DP has the capability to make metal parts directly from the CAD models using desired metal powders. In the past, parts have been created in a range of materials including stainless steel, tungsten, and tungsten carbide. However, the green parts produced by 3DP are delicate and must undergo further processing to achieve full density and desirable mechanical properties. The green part has typically 60% metal powder by volume, and the rest is void space.

Two alternatives for processing green parts are sintering the powder to its full density or infiltrating the void space with a lower melting temperature alloy. Figure 1.2 shows the example of each method. Figure 1.2(a) shows stainless steel parts sintered to full density in front of the initial green part to illustrate shrinkage. Figure 1.2(b) shows a larger (~15 cm part) skeleton before and after infiltration with bronze.

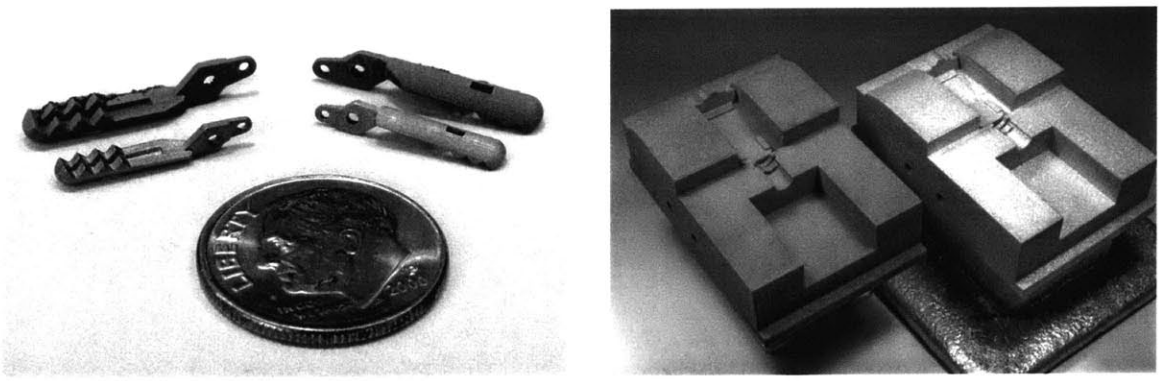

a) Sintered Part b) Infiltrated Part

Figure 1.2 Densification of green parts made by 3DP

Sintering powder to full density consists of heating the green part to near its melting point, causing the powder to consolidate by solid-state diffusion. This process has the advantage of creating a final part composition identical to the initial powder composition

as no additional material is added during densification. Therefore, materials choice is very good. But for the same reason, the powder skeleton undergoes significant dimensional change (~15%) during full-density sintering. So, typically it is only used for smaller (< 5 cm on a side) parts, for which shrinkage is uniform and distortion is not a problem.

The alternative method involves infiltrating the green part with a lower melting temperature alloy to fill the void space with negligible dimensional change. It makes this process a good choice for larger parts. For example, skeletons of stainless steel are usually infiltrated with alloys of copper. The final part, however, has a heterogeneous material composition, a mixture of powder material and lower melting temperature infiltrant. These composite materials, often have poor corrosion resistance and machinability and are not familiar to part designers.

Recently, a new process called transient liquid-phase infiltration (TLI) has been developed at MIT [3] for densification of powder metal skeleton without significant dimensional change, in contrast to full-density sintering, and that achieves a homogeneous final part composition, in contrast to traditional infiltration. This capability allows Solid Freeform Fabrication of large metal parts in an extended range of materials. In particular, the potential to match the final part composition to existing commercial alloys will be useful for critical applications (structural, aerospace, military), which require material certification.

1.3 Transient Liquid-phase Infiltration

Transient liquid-phase infiltration (TLI) is a densification process that uses an infiltrant similar to the powder material, but containing a melting point depressant, usually some common alloying element. Infiltration of green powder part is achieved by capillary action.

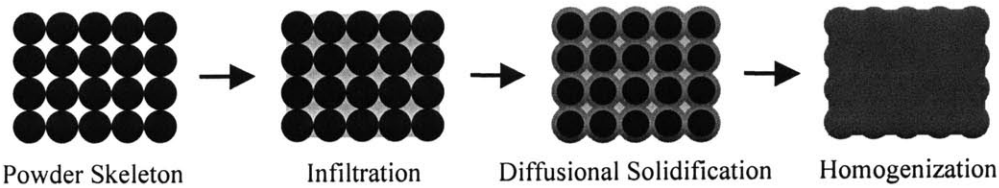

Figure 1.3 Schematic representation of TLI concept

Figure 1.3 shows the schematic representation of the TLI concept [3]. The molten infiltrant fills the porous powder skeleton in a time scale of few minutes. Over a longer period, as the melting point depressant diffuses into the base powder, the liquid undergoes isothermal solidification (or diffusional solidification) and the material eventually homogenizes. This process allows accurate dimensional control for larger parts with uniform or homogeneous material composition. The TLI process owes its name to the liquid-to-solid phase transition of the infiltrant during the diffusional solidification stage.

Figure 1.4 provides an example of TLI using a generic equilibrium phase diagram. The powder material in this case is pure metal A and the infiltrant is an alloy of metal A and a melting point depressant (MPD). At the infiltration temperature shown, *Ti*, the liquid infiltrant fills the void space of the skeleton achieving an average bulk composition that is not in equilibrium. The difference in MPD concentration between the infiltrant and skeleton causes isothermal solidification of the infiltrant as the MPD diffuses into the skeleton. This isothermal solidification is followed by homogenization and results in a final part composition equal to the average bulk composition after infiltration.

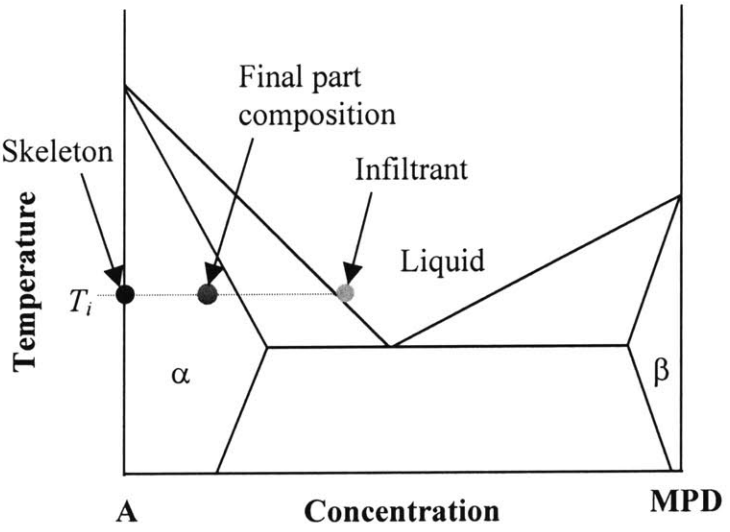

Figure 1.4 Generic phase diagram with labeled components of TLI

Lorenz [3] in his thesis has discussed the important issues of TLI in detail. The most important issue is the selection of infiltrant. The melting point depressant in the infiltrant is usually some common alloying element so that final part composition can be easily

matched with the existing commercial alloy of the metal. For example, silicon is used for nickel parts. Ideally, the MPD should be such that its diffusion in the base metal is slow enough to prevent premature freeze-off during infiltration, but fast enough to allow homogenization in reasonable time.

The concentration of MPD in the infiltrant is decided based on final material composition desired. For a skeleton containing no MPD with 40% void fraction, the concentration of MPD in the infiltrant should be ~2.5 times the desired final concentration, varying slightly if the skeleton and infiltrant densities are different. The infiltrant composition determines the minimum temperature at which liquid infiltration can occur. The final part microstructure and the degree of homogenization also depend on final bulk composition. If the final part composition is in the single equilibrium phase (Figure 1.4) then the final part will completely homogenize into a single solid solution. However, if the final bulk composition is in the two-phase field, then some liquid will remain at equilibrium until the part is cooled. This will result in two-phase microstructure of the final part. This could still be desirable in many cases.

The infiltration distance achieved in TLI is very much dependent on the material system used. Higher the diffusivity of MPD in the base material, faster will be diffusional solidification of the infiltrant resulting into early choke-off the infiltrant supply during the infiltration and hence less infiltration distance. Figure 1.5 illustrates how solidification chokes off the flow of liquid during infiltration, with an infiltrant supply completely cut-off in the third image, limiting the infiltration distance. For a given material system, infiltration height can be increased using metal powders of larger sizes, as fluid flow is faster in a bed of larger powder and solidification takes longer time to choke-off. An infiltration height of up to 22 cm has been achieved in nickel-silicon system using nickel powders of size over 300 microns [3].

Other issues in TLI include erosion of powder skeleton during infiltration and non-uniformity of composition throughout the part. In TLI, sometimes erosion of powder skeleton is observed because of the dissolution of the skeleton material in the liquid infiltrant when infiltrant is not saturated with base material. In addition, compositional non-uniformity can arise along the part if there is a change in liquid composition while

flowing the part. These issues can be addressed by some careful considerations like selection of proper infiltration temperature and is discussed in detail in [3].

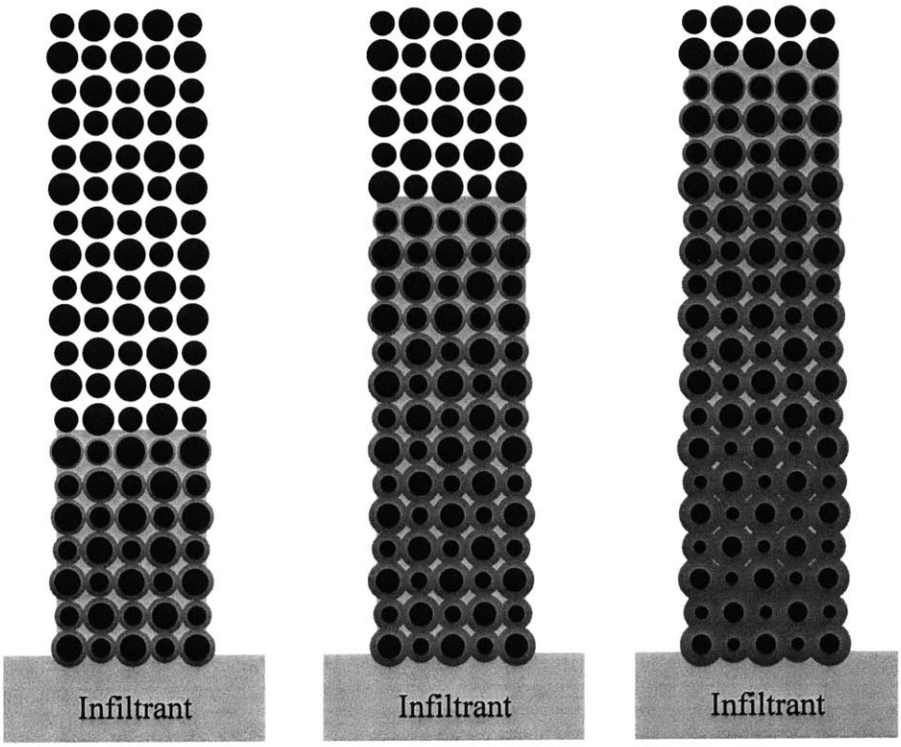

Figure 1.5 Infiltration of a powder skeleton with simultaneous diffusional solidification (progression from left to right) can cause freeze-off, limiting infiltration distance.

1.4 Previous Work

Initial work on transient liquid-phase infiltration was done by Lorenz [3], where he demonstrated the concept of TLI with Ni-Si model system. He analyzed the binary system in detail and explored various issues related with TLI. His work met with good success and it led to sound understanding of the physical concepts involved. In his experimental work using powders of various sizes, an infiltration height of up to 22cm was achieved.

Motivated with the success of the nickel system, the feasibility of TLI in aluminum system has been explored in this thesis. This will open up ways for free-form fabrication of aluminum parts directly from CAD models through powder route, which has several applications. As explained in the next chapter, earlier attempts in this direction has not

met with much success mainly because of the presence of thick and dense natural oxides on the surface of aluminum powder. Only Sercombe et al [5] has reported some success in free-form fabrication of functional aluminum prototypes using Extrusion freeform fabrication (EFF) process. They used liquid-phase sintering to consolidate green parts to near full density. In their work, they have illustrated fabrication of a small aluminum gear (~ 2cm diameter) with a metal-matrix composite wear surface.

This process however, cannot be easily scaled up to make large aluminum metal parts because of shrinkage and distortion issues involved with sintering process as mentioned in section 1.2. Therefore, it is necessary to develop a process, which will enable freeform fabrication of large aluminum metal parts directly from CAD models. This has been undertaken in this thesis.

1.5 Organization of Present Work

This work is organized in six chapters. The second chapter introduces various issues associated with the processing of aluminum powder in general and the specific challenges involved with transient liquid-phase infiltration of aluminum alloys. The chapter concludes with a feasibility test of TLI in aluminum. The subsequent chapters describe step-by-step procedures to overcome various challenges in the process. The third chapter explains the design and development of the experimental setup for infiltration of aluminum powder parts. It provides details for the design of the gettering system developed to achieve more controlled and oxygen free atmosphere for processing of aluminum. Chapter four explains that how the problem of oxide skin, both on the surface of infiltrant melt and on the powder preform, were overcome. Chapter five provides characterization of the infiltrated part and discusses various issues involved. Finally, chapter six concludes the thesis by summarizing the current work, and provides guidelines for future research in this direction.

Chapter 2. TLI with Aluminum: Background and Challenges

2.1 Motivation

The ability to make aluminum parts using SFF processes would create tremendous opportunities because of their combination of high strength, lightweight, corrosion resistance, and high thermal and electrical conductivity. Increased demand for lightweight components, primarily driven by the need to reduce energy consumption in a variety of components, has led to an increased use of aluminum these days. Additionally, the time required for making molds and their cost of fabrication coupled with the need for making design iterations have led to a significant emphasis on Solid Freeform Fabrication (SFF) processes, the ability to make parts directly from CAD models.

Fabrication of aluminum metal parts using SFF processes like 3DP and subsequent densification by Transient Liquid - phase Infiltration offer the conventional benefit of the 3DP process combined with the inherent advantages of aluminum and its alloys [2,15].

1. Parts of any shape and complexity can be produced directly from CAD models without going through the costly and time-consuming process of mold designing or manufacturing process planning. It has unprecedented flexibility with no geometric or tooling limitations. It can significantly reduce time to market for new products and enables a lot of quick and easy design iterations required for design optimization.
2. 3DP offers the potential for direct manufacture of structural components with unique microstructures and capabilities by locally tailoring the material composition, microstructure, and the surface texture.
3. Lightweight: Ever increasing demand for portable tools, equipments, and appliances such as power tools, farm and garden machines and copiers, electronic equipment – computers, etc., cameras and movie projectors, etc. – has increased the use of aluminum to make lightweight components. Automobile and aerospace industry has its own reason to prefer aluminum parts.

4. Corrosion Resistance: Unlike some iron and copper parts, aluminum parts usually don't require special handling and storage precautions. Natural corrosion resistance and popular optional treatments such as anodizing help in reducing the special handling requirements for parts.
5. Electrical and Thermal Conductivity: Compared to specific brass, bronze, and iron parts, aluminum alloys offer significantly higher conductivity. This enables the use of aluminum metal parts in heat transfer devices and in other electrical conductive parts.
6. Workability: Good ductility of aluminum metal parts permits sizing, coining, and restructuring operations to improve dimensional tolerances and upgrade properties.
7. Finishes: Appearance of parts can be enhanced by colorful anodizing process such as Alumilite. In addition, satin or matte and bright finishes are also possible.
8. Electrical Appliances: Non-magnetic properties of aluminum enable its utilization in the vicinity of electrical fields present in computers and in other electronic devices.

Though the ability to make aluminum metal parts using SFF process presents tremendous opportunities not much success has been reported in this field till date. The primary reason is that aluminum presents a unique challenge of handling its stable oxide during processing. Sercombe et al., [5] has reported some success in making small aluminum parts using Extrusion freeform fabrication process followed by liquid phase sintering.

Motivation for the present work is to develop a process that will enable production of fully dense direct aluminum metal parts from metal powder using SFF process like 3DP.

2.2 Aluminum Powder

Aluminum powder, produced by a variety of techniques, has physical and metallurgical characteristics related to its method of manufacturing and tailored to its end use. It is used in the manufacture of automobiles, commercial vehicles, aerospace, marine, railways, containers and packaging, cooking utensils, electronics, electrical transmission wire, telecommunications cable, paint pigment, metallurgy, batteries, energy storage, superconductors, construction industry, etc.

Aluminum powder is available in numerous granulation sizes and can be obtained from various sources within US. All the aluminum powders for current work were obtained from Alfa Aesar. Majority of the work were done with –40 +325 mesh (149 - 420microns) powder and sometimes with -100 +325 mesh (44 - 149 microns) powder. Their specified purity levels are 99.8 % and 99.97% (metals basis) respectively. Table 2.1 shows typical chemical analysis of –100 +325 mesh powder and

Table 2.2 shows its sieve analysis. Iron and silicon are major contaminants for aluminum powders.

Table 2.1 Chemical analysis of Aluminum powder

Element	Wt. Percentage	Element	Wt. Percentage
Al	99.87	Fe	0.0861
Si	0.0303	Mn	< 0.0010
Cu	0.0012	Zn	< 0.0050
Mg	< 0.0050	Cr	< 0.0050
Ni	< 0.0010	Sn	< 0.0050
Pb	< 0.0020	Na	< 0.0050
Ti	< 0.0020	V	< 0.0053
Sr	< 0.0005	Zr	0.0012

Table 2.2 Sieve analysis of –40 +100 mesh Al powder

Particle Size	Percentage
> 425 micron	1.0 %
>212 micron	30.0 %
>150 micron	63.0 %
> 106 micron	94.0 %
> 75 micron	98.0 %
< 75 micron	2.0 %

These powders were produced by air atomization process and are irregular in shape. Figure 2.1 shows the microphotograph of aluminum powder.

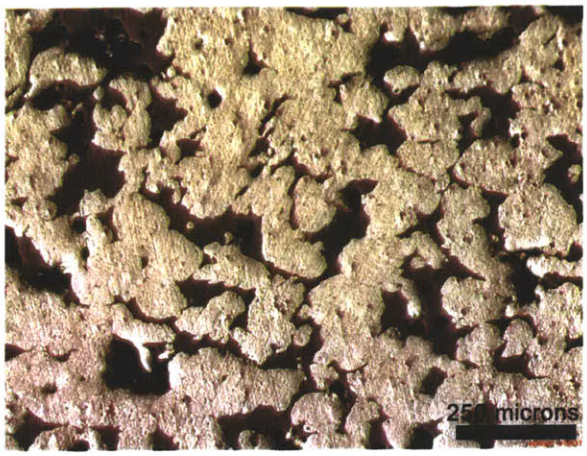

Figure 2.1: Microphotograph of Aluminum powder (-40 +100 mesh)

Aluminum powder is silver gray in color and is odorless. Table 2.3 shows the typical physical properties of atomized aluminum powder [1].

Table 2.3 Typical Physical properties

Wrought Density	2.7 g/cc (metal)
Melting Point	660 ^{0}C
Boiling Pint	2430 ^{0}C
Surface Tension at 800 ^{0}C	865 dynes/cm
Apparent Density	0.8 to 1.3-g/ cc (30-48 %)
Tap Density	1.2 to 1.5 g/cc (44-55%)
Melting Point of Oxide	2045 ^{0}C
Al_2O_3 content	0.1 to 1.0 wt %

The real density of aluminum powder approaches that of base metal, but both apparent density and tap density vary as a function of particle size distribution. The apparent density of –40 +325 mesh aluminum powder is 0.95 g/cc (35%).

Aluminum reacts readily with moisture or free oxygen in the air during manufacturing to form an oxide coating on the powder surface. Its oxide contents vary as a function of the

particle size and range from 0.1 to 1.0-wt %. Finer powders due to their higher surface area show highest percentage of oxide. Because the aluminum powder surface is hygroscopic, it also contains moisture in the form of physically absorbed water and hydrated aluminum oxide.

2.3 Overview of Aluminum alloys

In high purity form, aluminum is soft and ductile. It is typically used in electrical and chemical applications because of its high conductivity and excellent corrosion resistance. Most commercial uses, however, require greater strength than pure aluminum affords. This is achieved in aluminum by the addition of other elements to produce various alloys, which individually or in combination impart strength to the metal. Further strengthening is possible by means that classify the alloys roughly into two categories, non-heat-treatable and heat-treatable [1].

Heat-Treatable Alloys are those that can be hardened (strengthened) by a controlled cycle of heating and cooling. Some aluminum alloys, usually containing alloying elements such as copper, magnesium, zinc, and silicon are solution heat treatable. Since these elements in various combinations show increasing solid solubility in aluminum with increasing temperature, it is possible to subject them to thermal treatments that will impart pronounced strengthening. These treatments include heating and then quenching, or rapid cooling. They can be further strengthened by cold working – controlled deformation at room temperature.

Non-Heat-Treatable Alloys are hardenable by cold working, but not by heat treatment. The initial strength of alloys in this group is provided by the hardening effect of their alloying elements such as manganese, silicon, iron, and magnesium, singly or in various combinations. Additional strengthening can be created by cold working – deformation that induces strain hardening, denoted by H-tempers.

Principal alloying elements in aluminum are silicon, magnesium, copper, manganese, and zinc. Various other elements like tin, lithium etc. are also used sometimes to achieve desired effects. In this work, silicon and magnesium were used extensively and their effect on properties of the alloy is discussed next.

2.3.1 Aluminum – Silicon Alloys

Silicon is a very common alloying element in aluminum castings (3xx.x and 4xx.x series). In fact, Aluminum-Silicon castings constitute 85-90% of the total aluminum cast parts produced [8]. It is present in many wrought alloys as well (4xxx alloys). Additions of silicon to pure aluminum reduce its melting point and dramatically improve fluidity, hot tear resistance, and feeding characteristics. It also leads to a reduction in density and in coefficient of thermal expansion. So, Al-Si, alloys offer unique combination of desirable characteristics, including excellent castability, low density, good corrosion resistance, and good mechanical properties.

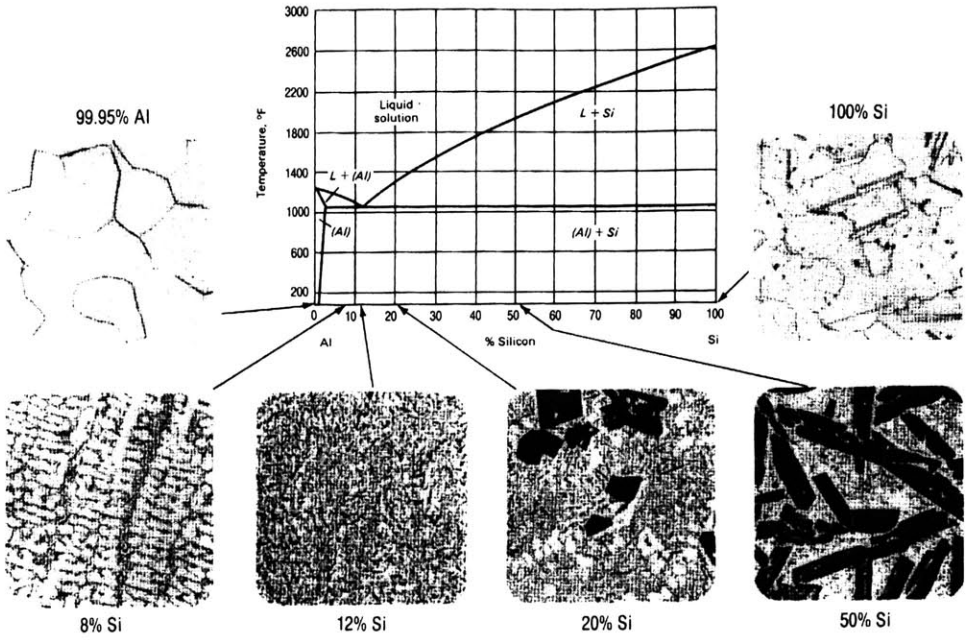

Figure 2.2 Al-Si Phase diagram and cast microstructure of pure components and alloys of various compositions

Aluminum-Silicon binary system is a simple eutectic alloy system with eutectic composition at 12.5% Si. Figure 2.2 shows the binary Al-Si phase diagram with microstructures of pure components and of several intermediate compositions (source [1]). The intermediate compositions are mixtures of aluminum containing about 1% Si in solid solution as continuous phase, with particles of essentially pure silicon. Alloys with

less than 12% Si are referred to as hypoeutectic, those close to 12% Si as eutectic, and those with over 12% Si as hypereutectic. Commercial alloys span the hypoeutectic and hypereutectic ranges up to about 25%. Standard alloys, of course, contain a number of other alloying ingredients as well.

At room temperature, the hypoeutectic alloys consist of the soft ductile primary aluminum phase and very hard, brittle silicon phase associated with eutectic reaction. It is this silicon phase that contributes to the very good wear resistance of these alloys. The silicon phase is diamond cubic with a density of ~ 2.6 g/cc and a Vickers hardness of approximately 10 GPa. Figure 2.2 (8% Si) shows the typical microstructure of a hypoeutectic alloy. Hypereutectic alloys, most commonly used wear-resistance alloys, contain coarse, angular, primary silicon particles as well as eutectic silicon. These primary silicon particles impart excellent wear resistance to the alloys. 20 % Si in Figure 2.2 shows the typical microstructure of hypereutectic alloy.

Strength and ductility of these alloys, especially those with higher silicon, can be substantially improved by modification of Al-Si eutectic. Modification of hypereutectic alloys is particularly advantageous in sand castings (involving slow cooling) and can be effectively achieved through the addition of controlled amount of sodium or strontium, which refines eutectic phase. Calcium and antimony additions are also used. Pseudo-modification, in which the fineness of the eutectic but not the structure is affected, may be achieved by controlling the solidification rates. In hypereutectic Al-Si alloys, refinement of the proeutectic silicon phase by phosphorous addition is essential for casting and product performance. Silicon particles become finer and more evenly distributed by the phosphorus treatment. A detailed discussion of microstructure modification is given in [1] and [8].

2.3.2 Aluminum Magnesium Alloys

Magnesium is another common alloying element in aluminum. It is the major alloying element in the 5xxx series of wrought alloys and 5xxx.x series of casting alloys. Its maximum solubility in aluminum is 17.4%. Figure 2.3 shows the binary phase diagram of Aluminum-Magnesium.

Binary Al-Mg alloys are characterized by high corrosion resistance, good machinability, and excellent appearance when anodized [8]. The addition of magnesium markedly increases the strength of aluminum without unduly decreasing the ductility [1]. So, they are widely used in applications requiring a bright surface finish and corrosion resistance, as well as attractive combination of strength and ductility. For example, they are used in seawater and marine applications. These alloys are suitable for welded assemblies and are often used in architectural and other decorative or building needs. Common compositions range from 4 to 10% Mg in casting alloys and never exceed 5.5% Mg in wrought alloys. Compositions containing more than 7% Mg are heat-treatable. Instability and room temperature aging characteristics at higher magnesium concentrations encourage heat treatment.

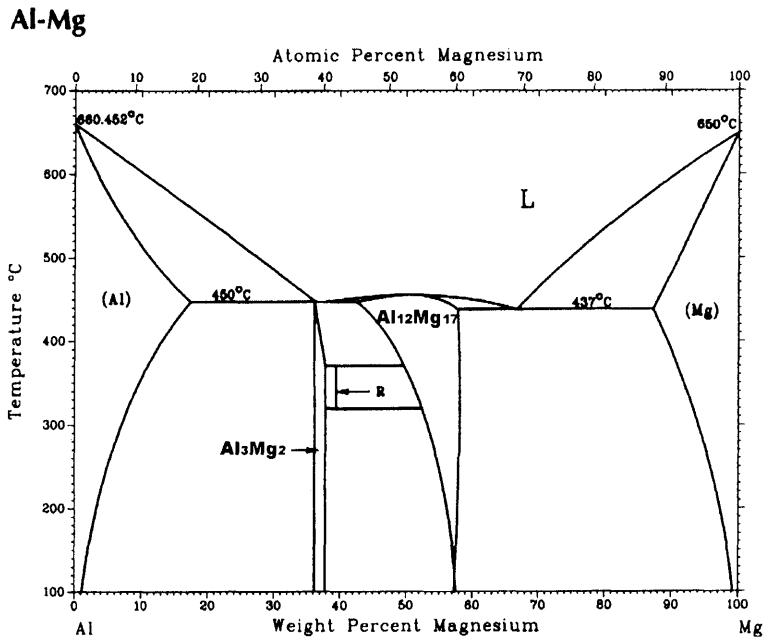

Figure 2.3 Al-Mg Phase diagram

In comparison to aluminum-silicon alloys, all the aluminum-magnesium alloys are generally more difficult to cast, since they freeze as a solid solution over a wide temperature range (Figure 2.3). Therefore, they require care in gating, good risering, and greater chilling to ensure sound castings. Magnesium increases the tendency for oxidation of the molten alloy and small additions of Be are often made to control the drossage.

2.3.3 Aluminum-Magnesium-Silicon Alloys

Aluminum-magnesium-silicon constitutes another important alloy group. It includes 6xxx group of wrought alloy and many alloys in 3xx.x casting series. The aluminum-silicon-magnesium system is represented by a pseudo-binary Al- Mg_2Si diagram in Figure 2.4.

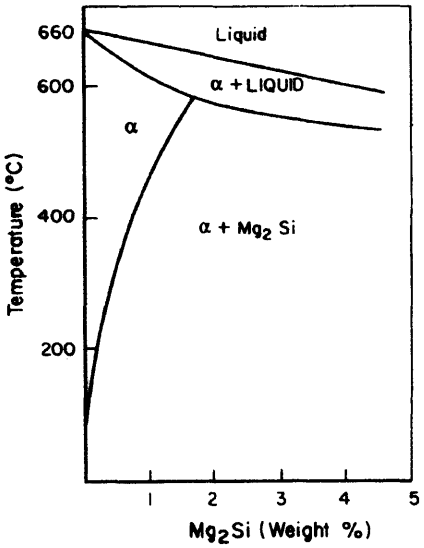

Figure 2.4 Al-Mg_2Si phase diagram

Magnesium is added in Al-Si alloys for development of strength and hardness through precipitation of Mg_2Si in the matrix. Its addition makes aluminum-silicon alloy heat-treatable. After solution treatment and quenching, aging results in uniform distribution of Mg_2Si precipitates throughout aluminum dendrites. It confers strength to these alloys. Figure 2.5 illustrates the typical microstructure of magnesium containing aluminum silicon alloy, A357.0 (Al-7Si-0.5Mg) [1]. The hardening phase Mg_2Si displays a useful solubility limit corresponding to approximately 0.7 % Mg (1.85% Mg_2Si), beyond which either no strengthening occurs or matrix softening takes place because excess magnesium over that required to form Mg_2Si sharply reduces the solid solubility of this compound.

Common premium-strength compositions in Al-Si family castings employ magnesium in the range of 0.40 to 0.070%. Wrought alloys contain up to 1.5% each of magnesium and silicon in the approximate ratio to form Mg_2Si, that is, 1.73:1. An excess of silicon in these alloys leads to increased strength. For example, an excess of 0.2% Si increases the strength of an alloy containing 0.8% Mg_2Si by about 70 MPa. Larger amounts of excess silicon are less beneficial. Excess magnesium, however, is of benefit only at low Mg_2Si

contents because Mg lowers the solubility of Mg_2Si. In excess silicon alloys, segregation of Si to the boundary causes grain-boundary fracture in recrystallized structures. Additions of manganese, chromium, or zirconium counteract the effect of silicon by preventing re-crystallization during heat treatment.

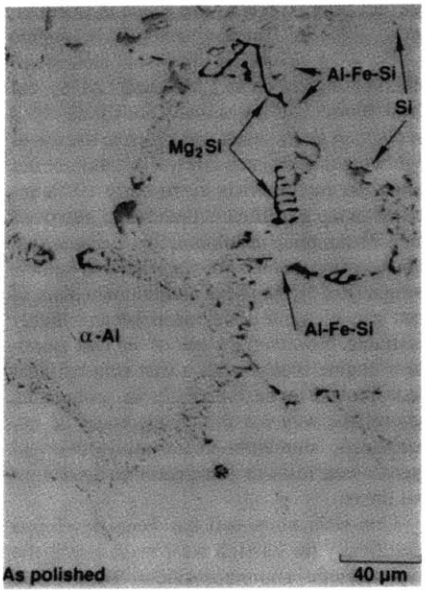

Figure 2.5 Microstructure of alloy A357.0 (Al-7Si-0.5Mg)

2.4 Oxide

Aluminum is a highly reactive element and it readily oxidizes even at room temperature. Therefore, a thin layer of oxide skin always surrounds aluminum powder particles. A lot of study has been done on the formation of oxide layer on aluminum and attempts have been made to determine its thickness. Sercombe [9] in his thesis presented a critical overview of it. The oxide layer thickness on air atomized Al powder has been reported to be of the order of 50 A°. However, the oxide skin is not uniform on the surface. There are islands of thick oxide skin on the surface of the powder that is formed during cooling (i.e. during atomization) and they are surrounded by thinner room temperature oxide.

These oxides are responsible for irregular morphology of the Al powder. According to proposed theories, when the oxygen potential of the atomizing gas is high, such as during air atomization, there will be many nucleation sites for oxidation. Each oxide nucleus on

the surface, being solid, will act as a pinning point, restraining surface tension forces, thereby resulting in irregular morphology.

The presence of oxide layer on Al powder prevents solid-state sintering. This has been explained in terms of the relative diffusion rates through the oxide and metal, for metals with stable oxides [11,27]. The stable oxide layer on aluminum reduces solid-state diffusion, therefore, needs to be reduced or otherwise removed to enable effective sintering. The oxidation of a metal (M) may be represented by [6]

$$M + O_2 \leftrightarrow MO_2 \qquad [2.1]$$

The free energy of formation (ΔG) of the oxide is given by

$$\Delta G = -RT \ln K_1 \qquad [2.2]$$

where R is the gas constant, T is the temperature in Kelvin, and K_1 is the equilibrium constant given by

$$K_1 = (P_{O2})^{-1} \qquad [2.3]$$

where P_{O2} is the partial pressure of oxygen when reaction [2.1] is at equilibrium. For aluminum at 600 °C a $P_{O2} < 10^{-50}$ atm is required to reduce the oxide [17]. Atmospheres containing hydrogen is often used in powder metallurgy to reduce oxides. Hydrogen can reduce a metal oxide by the reaction

$$MO + H_2 \leftrightarrow M + H_2O \qquad [2.4]$$

The equilibrium constant for this reaction (K_2) is given by

$$K_2 = P_{H2O} / P_{H2} \qquad [2.5]$$

where P_{H2} and P_{H2O} are the partial pressures of hydrogen and water vapor, respectively. The ratio of partial pressures can be converted to dew point, which is effectively the water vapor content. A dew point of $\leq$ -140 °C at 600 °C is required to reduce Al_2O_3 [17]. Neither a dew point of -140 °C nor a P_{O2} of 10^{-50} atm is practically attainable; therefore, aluminum oxide cannot be reduced by conventional means.

Another problem with the oxide is that liquid aluminum doesn't wet its oxide. The wettability of a solid by a liquid is determined the work of adhesion (W_a) [6]:

$$W_a = \gamma_{lv}(1+\cos\theta) = \gamma_{sv} + \gamma_{lv} - \gamma_{sl} \quad [2.6]$$

where γ_{lv} is the surface tension of the liquid, γ_{sv} is the surface tension of solid-vapor interface, γ_{sl} is the solid-liquid interfacial tension, and θ is the contact angle. A liquid is said to wet a solid when $\cos\theta > 0$, or $\theta < 90^{o}$. The contact angle of liquid aluminum on aluminum oxide has been reported to be ~103 deg at 900 °C [25] or ~ 160 deg at 800 °C [26]. This non-wetting behavior of aluminum on its oxide causes problem for liquid-phase sintering [6] and will prevent any infiltration as well.

It is, thus apparent that aluminum oxide is an obstruction for getting fully dense aluminum metal parts through powder route either by sintering or by infiltration and must be disrupted to achieve fully dense parts.

2.5 TLI with Aluminum

As discussed in chapter 1 Transient Liquid-Phase Infiltration (TLI) is a process developed at MIT to densify inherently porous 3D printed metal part or more generally, any green part produced by powder metallurgy processes. TLI in aluminum can be achieved by infiltrating pure aluminum powder skeleton with its alloy having lower melting point.

2.5.1 Selection of Infiltrant

The appropriate selection of infiltrant is very crucial in TLI as the infiltrant will stay in the part and will affect final part composition and its properties. The infiltrant in TLI is primarily the same metal as that of the skeleton but contains some melting point depressants (MPD) to lower its melting point. Aluminum offers many potential melting point depressants for use in an infiltrant. Table 2.4 summarizes the effect of commonly used alloying elements on the melting point of aluminum. Pure aluminum has a melting point temperature of ~ 660 °C. Ternary and quaternary alloys can provide additional melting point depression. For example, an aluminum alloy 336.0, commonly used in die casting of automotive pistons, containing 12Si–2.5Ni–1Mg–1Cu has a solidus of 540°C and a liquidus of 565°C.

Table 2.4 Effect of various alloying elements on the melting point of aluminum

Alloying Element in Aluminum	Eutectic Comp (wt%)	Melting Point (°C)	Melting point depression (°C)
Silicon (Si)	12	577	83
Magnesium (Mg)	35	450	210
Copper (Cu)	30	548	112
Germanium (Ge)	50	420	240
Lithium (Li)	8	596	64

.

We chose to work with Al-Si system as an infiltrant because silicon offers high melting point depression at lower concentrations. In addition, silicon is extensively used as commercial alloying element for Aluminum. Figure 2.6 shows the aluminum rich side of the Al–Si binary phase diagram. A 60% dense skeleton of pure aluminum infiltrated with Al–10Si at 600°C would have a final part composition of 4% Si. Since this composition lies in a two-phase region on the phase diagram, it means that the infiltrant will not completely solidify at the infiltration temperature. Based on lever rule, it will have 75% solid and 25% liquid at 600°C. Therefore, the skeleton would absorb some Si, but isothermal solidification will occur only until the part is 75% solid.

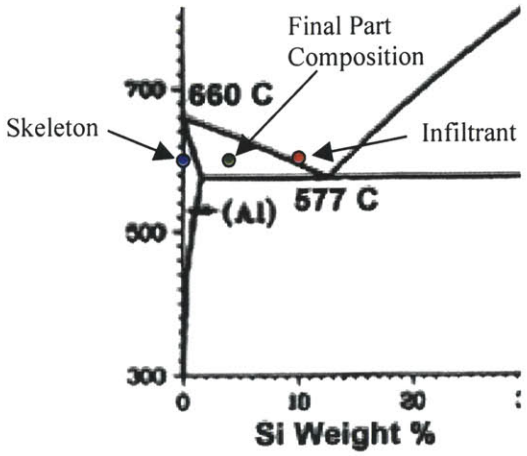

Figure 2.6 Al-Si Phase Diagram

The diffusivity of silicon in aluminum is ~1.5 x 10^{-12} m^2/s at 600°C. This results in a characteristic diffusion distance of ~20 μm in one minute. Because of the faster mass transport, this material system would be more prone to choke off the liquid flow if it were not for the low solubility of silicon in aluminum. The lower solubility would result in liquid flow never being choked off as long as the MPD final bulk composition is greater than the MPD solidus composition.

The final microstructure resulting in these cases of low solubility will not be a single-phase solid solution of the MPD in the skeleton material. The original void space that was filled with liquid will have a two-phase microstructure. This would resemble that of a cast microstructure. The powder particles that have absorbed Si would take the place of the primary dendrites that solidify first in a casting. The remaining infiltrant would have a eutectic microstructure similar to the sections of a casting between the dendrites that are the last to freeze. Since this type of microstructure is still desirable and widely accepted in industry, the fact that the material composition is not uniform throughout is not a drawback. Two-phase strengthening is common for commercial net-shape casting alloys and can be achieved in such cases of infiltrated systems with low solubility.

2.5.2 Proof of Concept

In the beginning, some experiments were done to test the feasibility of TLI in Aluminum. Experiments were conducted with 4047 - Al, a commercial brazing alloy containing 11-13 % Si, as infiltrant in a gold tube furnace with nitrogen atmosphere. Initial attempts to carry out infiltration in conventional way didn't work because of dense, stable oxide layer present on both aluminum powder skeleton and infiltrant. Infiltration was then tried by putting infiltrant under loose aluminum powder in a ceramic crucible. The idea was to bring the infiltrant and the aluminum powder in contact, in a very clean atmosphere as any oxygen present will react with the aluminum powder at the top surface and the interior of crucible will be practically free of oxygen. The loose powder skeleton infiltrated successfully to 93.5% density (Figure 2.7) except for the top surface, which was oxidized. This brought us to believe that TLI is feasible in Al but with a challenging task of taking care of oxides.

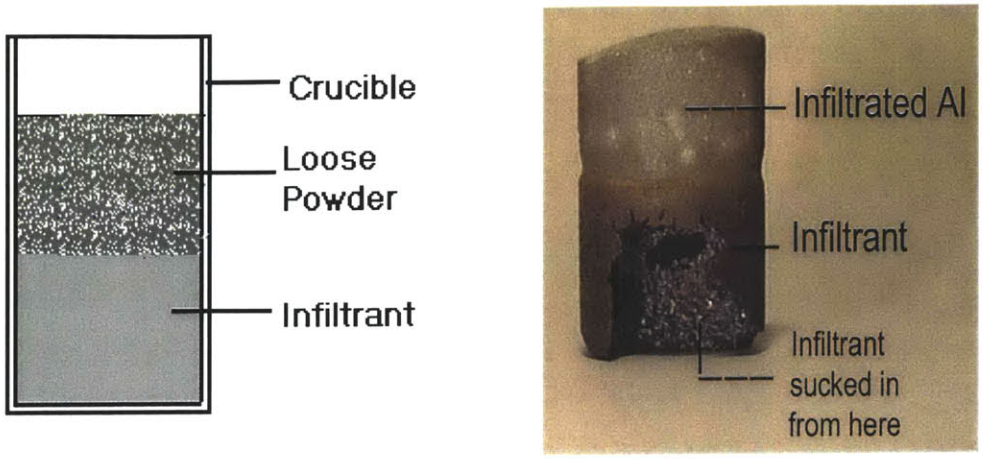

Before infiltration

After Infiltration

Figure 2.7 Infiltration experiment with Aluminum

2.5.3 Challenges and Approach

One challenge for TLI in aluminum is to conduct infiltration within a narrow temperature window, since the melting point depression of the infiltrant may be less than 100 °C. Fortunately, the lower operating temperature of aluminum allows for easier manipulation of the part and the melt.

Another challenge, which is very crucial for the successful processing of aluminum alloys, is the presence of natural oxides on the surface of both the powder skeleton and the infiltrant melt. As discussed earlier, these oxides prevent wetting of the skeleton by the infiltrant. Moreover, these oxide skins grow faster at higher temperature. This worsens the problem and so it is necessary to process aluminum in very clean atmosphere and somehow break the already existing oxide skin. This requires three major tasks:

Make the furnace atmosphere very clean.
Remove oxide from the surface of infiltrant melt.
Break the oxides on Aluminum Skeleton.

The subsequent chapters describe the step-by-step procedures adopted to overcome these challenges.

Chapter 3. Design of Experimental Apparatus

3.1 Furnace

Since aluminum is a very reactive element and oxidizes very easily, it is very important that it is processed in a very clean furnace, free of oxygen, water vapor, and any other contaminating elements. All the experiments in this research work were carried out in a gold tube furnace. Figure 3.1 shows the gold tube furnace. A schematic of it is shown in Figure 3.2

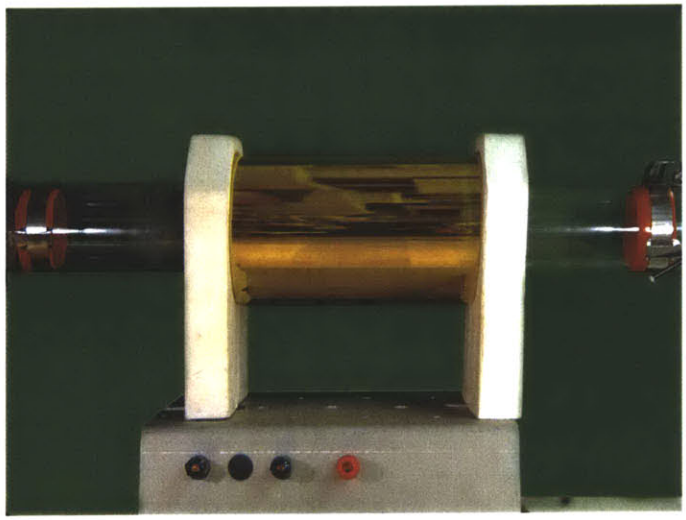

Figure 3.1 Gold Tube Furnace

Unlike conventional furnaces, the gold tube furnace uses a gold mirror for insulation and is transparent. Its main body consists of a glass tube with a gold film deposited on the inside surface. Inside of the gold coated tube is cemented, coaxially, a quartz tube. The purpose of the quartz is to keep the gold mirror clean. If the mirror is not clean then it will not reflect the radiation coming from the elements efficiently. The heating element is a coil-like structure that fits inside the mirror assembly. Finally, the working tube (muffle), made of quartz, slides inside the element. Each end is held in place by ceramic ends that are mounted on a base.

The gold mirror acts as insulation by reflecting back most of the radiation inside the furnace. At high temperatures, however, some radiation does escape through the mirror

and produce good view into the furnace, making it transparent. This enables accurate viewing of the samples inside the furnace, thermocouple placement, and process procedures. Due to use of only gold mirror as insulation and quartz working tube, the furnace is very clean as there is no contaminating fiber insulating material. This is very important for processing of aluminum as mentioned earlier. The use of gold insulation has an added advantage that the furnace has very low thermal mass and this makes it heat up and cool down very quickly. This again is beneficial for processing of aluminum as it minimizes the time for which samples stay at high temperatures and hence, minimize the further oxidation of samples as reaction kinetics are fast at high temperatures and samples are more prone to oxidation.

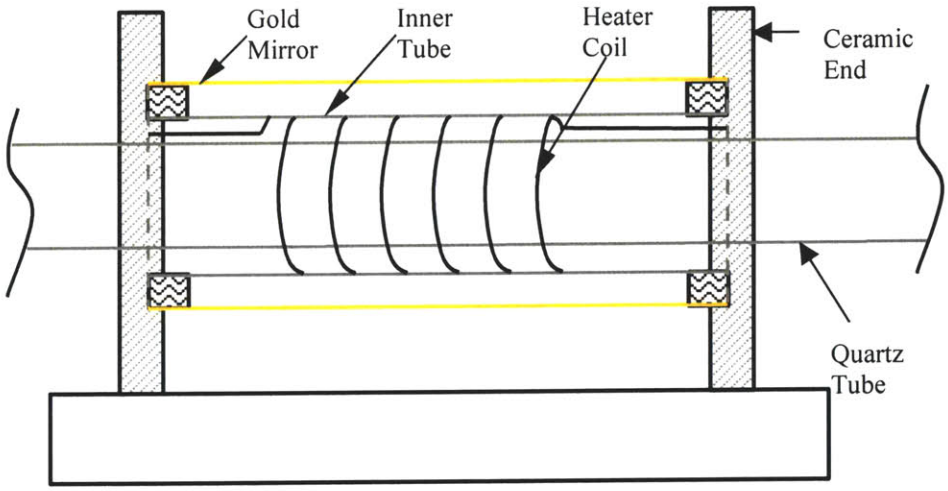

Figure 3.2 Schematic of Gold Tube Furnace

3.2 Furnace Atmosphere Control

It is a common practice to use inert atmosphere or vacuum inside the furnace for high temperature processing of metal parts. This is usually done to avoid oxidation of parts at high temperatures and sometimes to reduce already existing oxides. Nitrogen, dissociated ammonia, hydrogen, argon, and vacuum have been used for high temperature processing of aluminum powder metal parts like in sintering. However, nitrogen is preferred amongst these because it has been found experimentally that it results in high as-sintered mechanical properties [15,1]. In a patent literature [7], it has been suggested that nitrogen

in presence of magnesium helps in reduction of aluminum oxide, facilitating sintering. If a protective atmosphere is used, a dew point of –40°C is recommended [1]. This is equivalent to a moisture content of 120 mL/m^3 (120 ppm) maximum.

All the experiments in the current work were, therefore, done in a nitrogen atmosphere. Ultra high purity N_2 gas (Grade 5) supplied by BOC gas is used. Its purity level is 99.999% and has a maximum impurity of 10 ppm (O_2 < 3 ppm, H_2O < 5 ppm). Figure 3.3 shows the schematic of gas flow circuit for the gold tube furnace. Controlled amount of N_2 is let into the furnace from a gas tank using a pressure-regulator and a flowmeter. The ends of the furnace are sealed using end-caps with rubber gaskets to avoid any leakage. The outflow from the furnace is connected to exhaust duct through an exhaust valve. A pressure gauge along with a needle valve is provided at the furnace outlet to monitor and maintain appropriate pressure inside the furnace. A slight positive pressure of 8-10 inches of water is usually maintained. Provisions are made at the outlet to measure dew point of the furnace atmosphere. All the piping is done using flexible Teflon tubing to facilitate easy removal of end caps while loading and unloading the samples inside furnace.

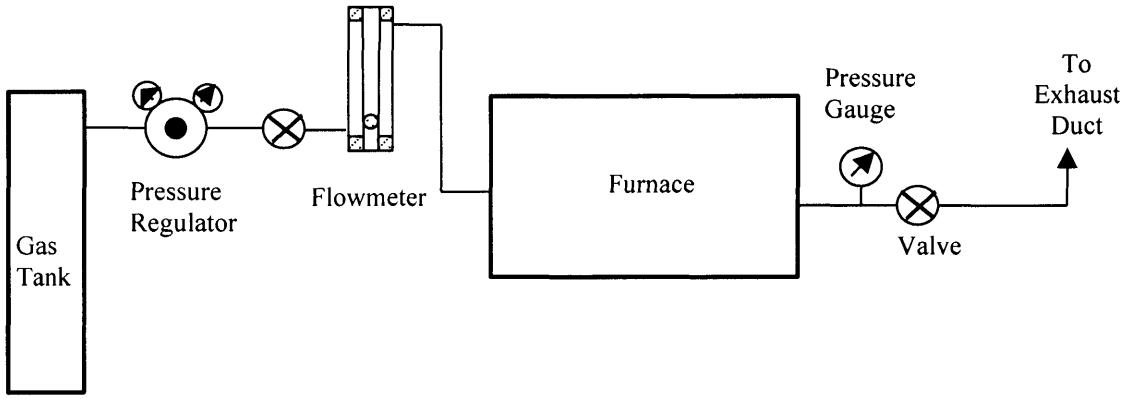

Figure 3.3 Schematic of gas system for gold tube furnace

Appropriate flow rates of nitrogen gas required for the furnace can be easily calculated from the volume of the furnace and the number of volume changes required per hour. A flow rate of 2 cfh of nitrogen is used in the furnace. The volume of its working tube is 87.4 cubic inch (~ 0.05 cubic ft). Therefore, a flow rate of 2 cfh results into 40 volume changes per hour.

3.3 Initial Attempts

With the given setup, some initial experiments were carried out both for sintering and infiltration. Sintering of loose powder was attempted at various temperatures from 500 °C to 650 °C to make a lightly sintered preform for infiltration. In all the experiments, even though a dew point of less than -40 °C was maintained, as suggested in handbooks, no sintering was achieved. Infiltration was attempted by putting infiltrant, 4047 Al (containing 11-13% Si), on the top of lightly pressed aluminum powder discs (~ 65 % dense). The samples were kept at 625 °C, well above the liquidus temperature of the infiltrant, for 30 minutes but no infiltration was observed.

Figure 3.4 shows the result of a typical such experiment. The lack of success in these experiments can be attributed to oxides as discussed earlier. In conventional sintering of powder metallurgy parts, these oxides are disrupted during compaction, which exposes the fresh surface, forms physical contact with a neighboring powder particle and enables sintering. However, in SFF processes, there is no compaction to rupture oxide films and hence the problem is more severe. This explains the failure of these experiments. Therefore, it is compulsory to carry out the experiments in more controlled composition atmospheres than required for conventional sintering. This necessitated a need to make the furnace atmosphere as clean as possible.

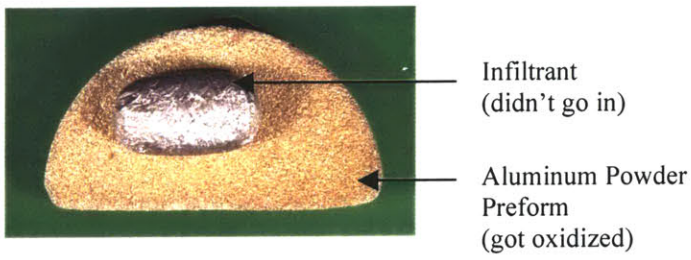

Figure 3.4 No infiltration in Aluminum Powder Preform

3.4 Gettering Mechanism

Making the furnace atmosphere clean is very important as it will minimize the further oxidation of aluminum parts while processing and possibly reduce some of the existing oxides. One of the methods for purification of the furnace atmosphere is using a gettering

agent in the furnace. The selective removal of one or more chemicals from a gas mixture by chemical reaction is commonly called gettering.

The gettering process for removal of oxygen involves using a reactive material, the "getter" (typically a metal), and allowing the process gas, which contains oxygen impurities to contact the hot getter. A chemical reaction occurs in which the oxygen forms a stable compound with the getter. If an oxide compound is a solid at the temperature of operation, then some amount of oxygen impurity is removed from the gas stream. The choice of proper temperature of the getter is based on several factors. These include the stability of the compounds formed, compatibility of the getter and its container, and the diffusion rate of the impurities in the getter material as a function of temperature.

Commercially available gettering furnaces use titanium and copper as gettering agents for oxygen. But both the elements are less reactive than aluminum. So the possibility of them working effectively with aluminum is doubtful. Moreover, that would require a separate gettering furnace, as their effective working temperature is different than our desired processing temperature of around 625 ^{o}C. So, it was decided to use aluminum itself, or some more reactive element than aluminum like magnesium, as a gettering agent. The idea was to place a disc made of highly reactive coarse metal powder upstream in the hot zone so that any oxygen present in the gas would react with the upstream reactive metal before it enters the work zone and hence provide clean atmosphere. Experiments were done with both Al and Mg and both gave similar performance. Aluminum was then preferred over magnesium because it is easier to work with it and it can be easily pressed into a disc. An additional advantage of using aluminum is that gettering can be done in the same furnace. This is very similar to the initial work on aluminum with infiltrant buried under powder. A setup was designed and built to implement the idea.

3.4.1 Design of Gettering System

Figure 3.5 shows the schematic of setup designed to use aluminum as a gettering agent. It consists of a stainless steel tube, which goes all the way into the hot zone. A porous disc made of pressed aluminum powder is placed in the hot zone end of the SS tube. It is very important that a good seal is maintained between the Al disc and the SS tube so that all

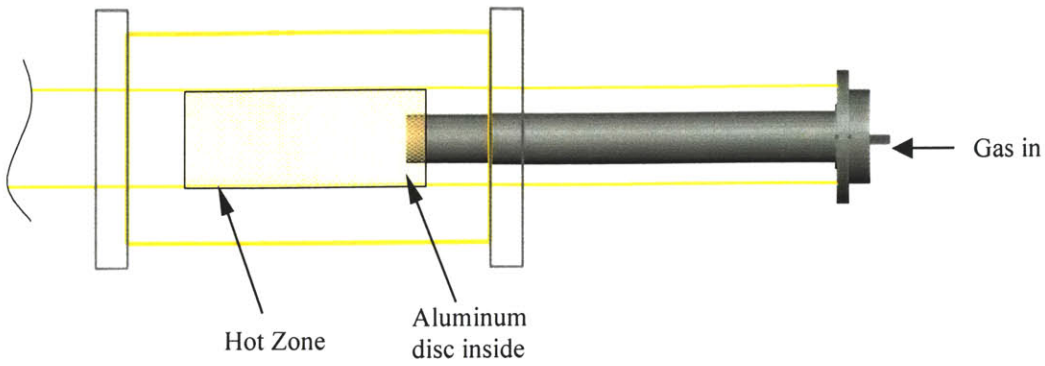

Figure 3.5 Schematic of Aluminum Gettering System

the process gas passes through the porous Al disc and doesn't escape from the sides. This seal is achieved by pressing the aluminum disc in the tube itself. Approximately 6g (results in ~ ¼" thick disc) of coarse aluminum powder is put inside the SS tube and pressed at its end in the arbor press using a ram made of stainless steel rod. During pressing a good seal is established between the tube and the pressed disc. The other end of the SS tube, which comes all the way out of the furnace, is welded to the end cap. The end cap has a through hole in its center to allow insertion of the ram inside the SS tube for pressing Al disc in it. This hole is plugged using another smaller end cap. The two end caps are closed and sealed together using an O-ring and three bolts. The smaller end cap has a pipefitting attached to it for gas inflow. Figure 3.6 shows the exploded view of the gettering system. A step has been provided on the SS tube to remove material from it in order to minimize conductive heat loss through the tube. Provisions have been made in the end caps to insert a thermocouple into the furnace.

Process gas from the gas tank enters into the furnace through the SS tube. This forces all the gas to pass through the porous aluminum disc before entering into the furnace. This disc acts as a getter. When the furnace is hot, any oxygen present in the gas inflow is exposed to the aluminum disc first and reacts with it to form aluminum oxide. As a result, the gas entering the work zone is virtually free of oxygen.

The getter charge (pressed aluminum disc) needs to be changed before every experiment as during the processing it gets lightly sintered, and shrinks a bit resulting into loss of its sealing with SS tube.

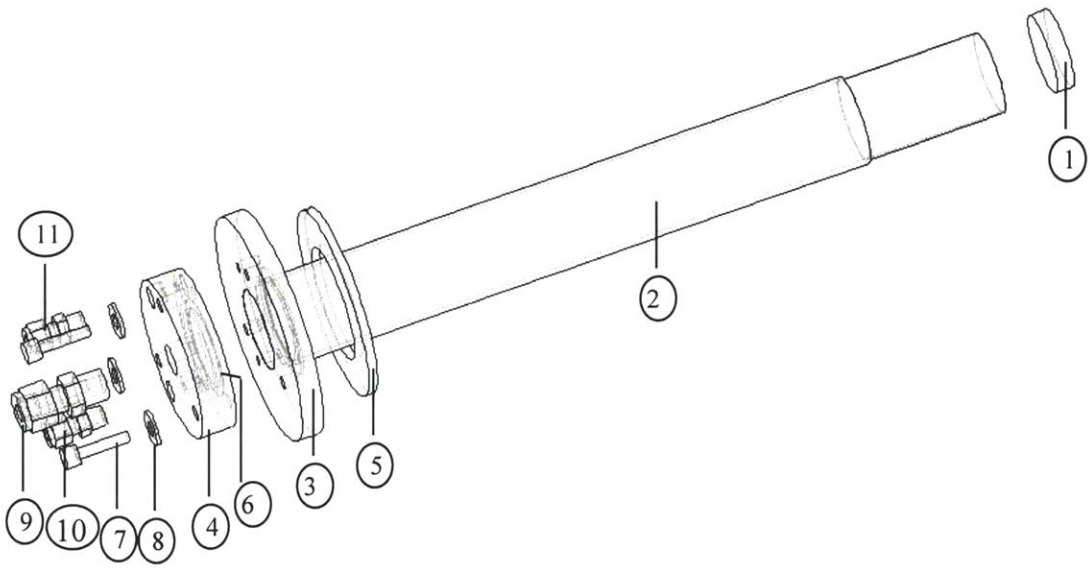

1. Getter Charge
2. SS Tube
3. End Cap
4. End Cap II
5. Gasket
6. O-Ring (not visible)
7. Bolts
8. Washer
9. Pipe fitting (for gas)
10. Pipe fitting (for Thermocouple)
11. Pipe fitting (auxiliary outlet)

Figure 3.6 Exploded view of Gettering System

3.4.2 Design of Heat Shield

The length of the working tube (quartz muffle) is 22 inches, but the length of the heating element is only 3 inches. A heat shield is used on both ends inside the working tube in the tube furnace to confine the hot zone within the heating element area only. It ensures a good uniform temperature profile inside the hot zone by restricting radiation losses to sides. It also helps in confining convection pattern of hot gases to the hot zone only and prevents direct escape of hot gases to the outlet. This is again helpful in maintaining uniform temperature inside the hot zone.

Figure 3.7 Heat shield for gold tube furnace

Figure 3.7 shows the heat shield made for the gold tube furnace. It consists of two discs made out of SS sheets and separated by small bolts. It is designed to have clearance fit with the working tube. A hole is provided in the center as restricted gas outlet. Additional holes have been made to allow insertion of various things like a thermocouple into the hot zone from outside.

3.4.3 Dead Zone and Gas Circulation

With the use of the designed aluminum gettering system, process gas enters the furnace directly into the hot zone and comes out from the other end. As a result, effective gas circulation occurs from hot zone onwards only and space before hot zone is dead zone (Figure 3.8). There is no gas re-circulation on this area. So when the furnace is purged with nitrogen, the air in this dead zone doesn't get flushed out from the furnace and oxygen content in the furnace doesn't go down very much even with the use of the gettering agent. Therefore, it is important to have good circulation of the gas in the entire furnace to drive out most of the air from the furnace.

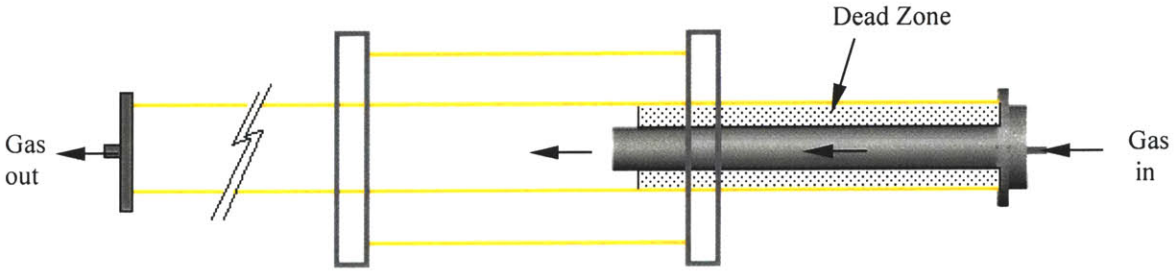

Figure 3.8 Gas flow in furnace and dead zone

The gas circulation system was hence redesigned to enable effective circulation of gas in the entire furnace. Figure 3.9 shows the schematic of new gas circulation system. It consists of two gas outlets, one main outlet at the exit, and another auxiliary outlet at the entrance of the furnace. Gas entering into the hot zone is forced to come out from both the ends. As a result, there is good circulation of gas in the entire furnace. The amount of gas coming out from both the ends is controlled by a flowmeter provided at the auxiliary outlet and a needle valve at the main outlet. A flow rate of ~ 0.5 cfh out from the auxiliary outlet is maintained in all the experiments. The rest gas (~ 1.5 cfh) comes out from the main outlet.

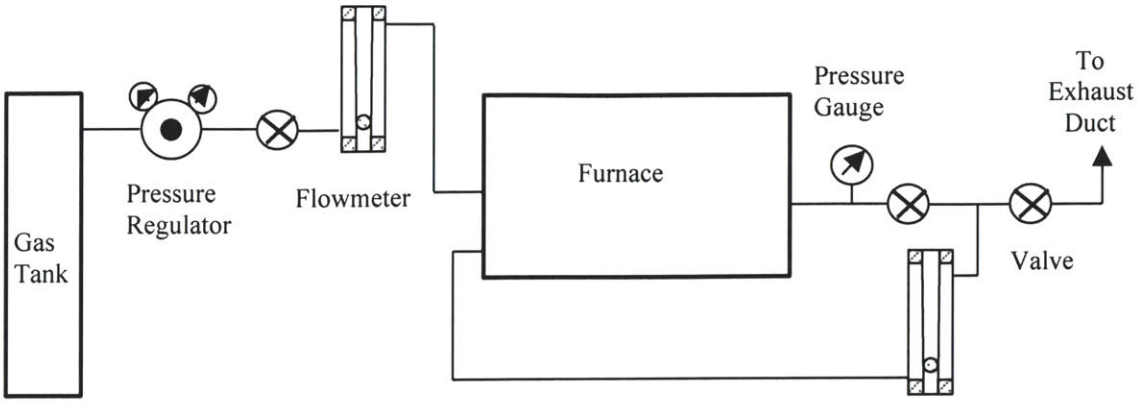

Figure 3.9 Modified gas flow system for gold tube furnace

3.5 Test of Setup

Infiltration experiments were conducted with this setup in the usual manner by putting infiltrant on the top of a lightly pressed aluminum powder preform. Figure 3.10(a) shows the sample after it was kept at 625 °C for 30 min. All the infiltrant got sucked in, implying successful infiltration. Moreover, there was no oxidation of the aluminum sample and the part came out very clean. On the other hand, the gettering charge was severely oxidized (Figure 3.10b). This means that aluminum disc is effectively acting as a getter.

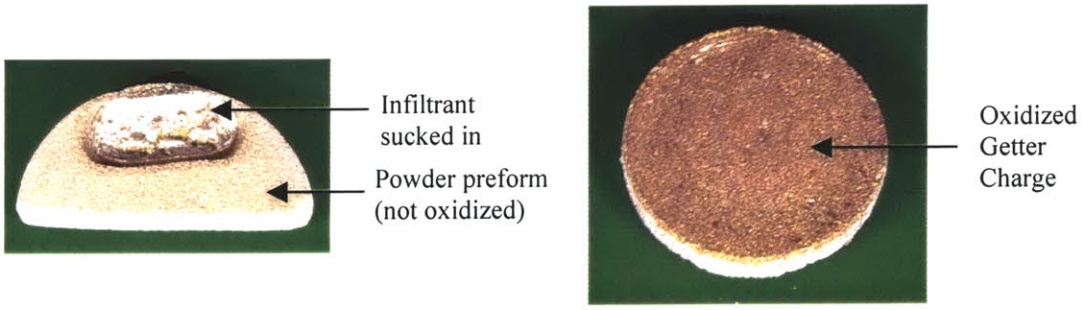

a) Infiltrated Part **b) Getter Charge**

Figure 3.10 Successfully infiltrated part and oxidized getter charge

3.6 Gated Infiltration

The infiltration experiments as described earlier, i.e. carrying out infiltration by putting infiltrant on the top of aluminum powder skeleton was good for testing purposes, but a real part cannot be infiltrated that way. Since alloys don't have a single melting point and

melt over a range of temperatures, the infiltrant will start melting even before achieving desired infiltration temperature. At different temperatures, the composition of liquid is different, decided by the tie line in the phase diagram corresponding to that temperature. For example, in Al-Si binary system liquidus composition at 600 °C is 10 wt% Si and at 625 °C it is 6 wt% Si. Therefore, infiltration will start even before the steady state temperature is achieved, and at different temperatures, liquids of different composition will infiltrate. This will lead to compositional inhomogeneity and it will be difficult to control the final composition of the infiltrated part. Thus it is desired that the powder preform is brought in contact with infiltrant melt only when the furnace and hence the infiltrant melt has reached the desired steady state temperature. This can be achieved a by gated infiltration of the parts.

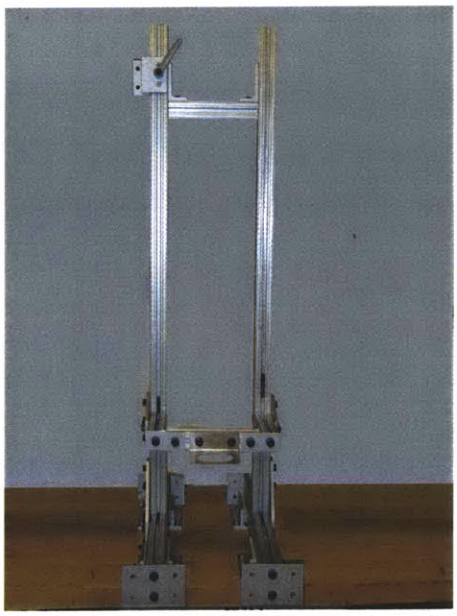

Figure 3.11 Sliding structure for gold tube furnace

There are many ways in which a gated infiltration can be carried out with real parts. The simplest way for experimental purposes is to hang the powder preform from a wire above a crucible containing infiltrant and dip it into the melt only after the infiltration temperature is achieved. However, this can be done only in a vertical tube furnace. So, the existing horizontal gold tube furnace was made vertical by mounting it on a vertical structure. Figure 3.11 shows the structure used for mounting the gold tube furnace

vertically. It is made of 1.5" x 1.5" T-slotted aluminum extrusions. All the necessary extrusions and joining plates were obtained from 80/20 inc. and were assembled into a sliding structure on the worktable. The structure was made sliding to facilitate easy mounting and dismounting of the 10-inch long end cap from the bottom without making the structure unnecessarily tall. During mounting (or dismounting) the structure is brought forward so that the working tube is out of table edge and the end cap can be easily inserted (or removed) from bottom. Once assembled the whole structure is slid back to the original position on the table. The sliding structure is achieved through two pairs of linear bearings.

In the vertical gold tube furnace, nitrogen gas is fed from the bottom and the main outlet is at the top. Crucibles and samples are supported inside the hot zone on a three-legged small SS structure (Figure 3.12), which rests on the step of SS tube of the gettering system. The discoloration of the SS structure happened initially because of oxidation when there were leaks in the furnace, which were removed subsequently. The bottom heat shield is also rested at the same step below SS support. The top heat shield is hanged from the top end cap using two 1/8" rods.

Figure 3.12 SS structure to support samples inside furnace

The gated infiltration is carried out by hanging the aluminum preform from the top end cap using a 0.010"∅ molybdenum wire and a 1/8" SS rod. The sample is attached to molybdenum wire, which in turn is attached to the SS rod. The SS rod comes out through the end cap and is secured and sealed in place using a pipefitting with Teflon ferrules. For dipping, the pipefitting is simply loosened and rod is slid into the furnace by the desired amount. The detail diagram of the dipping mechanism is shown in the next chapter (Figure 4.4). Figure 3.13 shows the complete setup used for the TLI experiments.

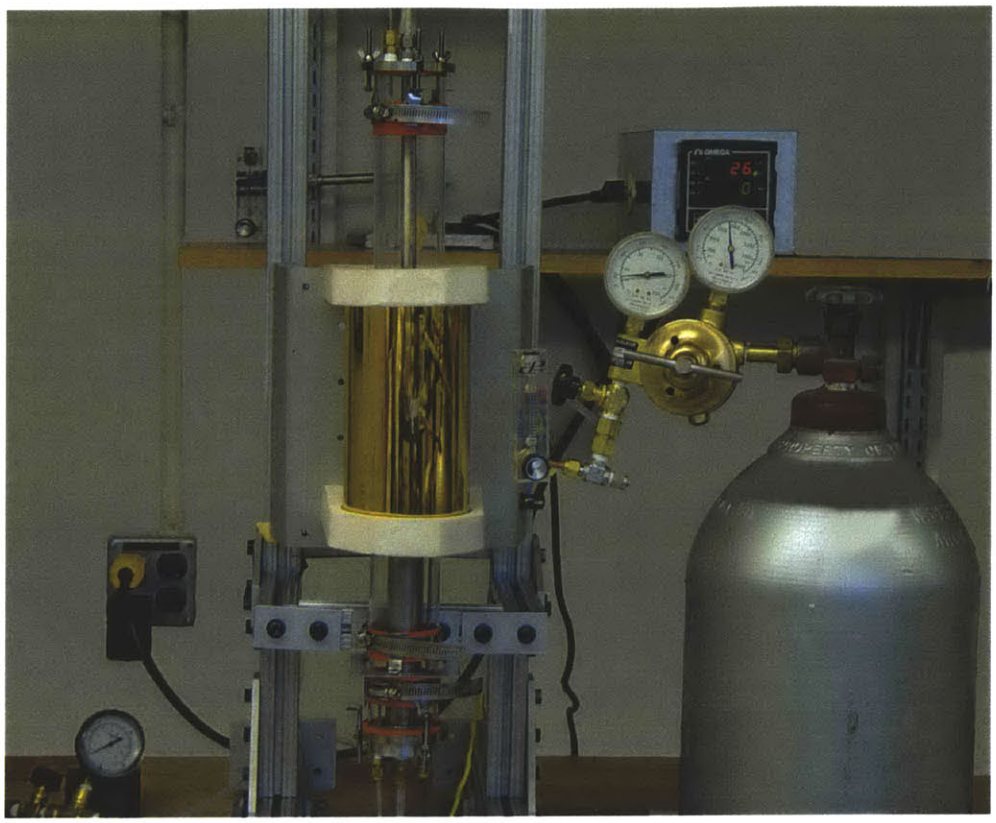

Figure 3.13 Complete setup for TLI of aluminum alloys

3.7 Crucible

All the infiltration experiments were done in a graphite crucible. Figure 3.14 shows the graphite crucible used for gated infiltration experiments. Graphite was chosen as crucible material because liquid aluminum metal and its alloys doesn't wet graphite and hence doesn't stick to the crucible after solidification. Alumina ceramic crucible, commonly used in high temperature processing, couldn't be used because liquid aluminum especially one containing magnesium sticks to it after solidification.

Figure 3.14 Graphite crucible

3.8 Hot Zone

The hot zone of the gold tube furnace was initially 3 inches. It was sufficient for initial infiltration experiments, but with the use of the aluminum gettering mechanism, it was not enough for gated infiltrations. It was difficult to get even one-inch tall sample completely into the hot zone for a gated infiltration. Therefore, the length of hot zone was increased by replacing the heating element with a new longer one.

New heating element was obtained from Thermcraft Inc. and was installed into the gold tube furnace. Table 3.1 shows the specification of the new heating element.

Table 3.1 Specification of Heating Element

Length	4.5"
Internal Diameter	2.75"
Power	600 Watts
Voltage	110 Volts
Resistance	16 Ohm
Zone	One

The furnace was characterized with the new heating element. Figure 3.15 and Figure 3.16 represents the furnace's fast heating and cooling rate with the new heating element.

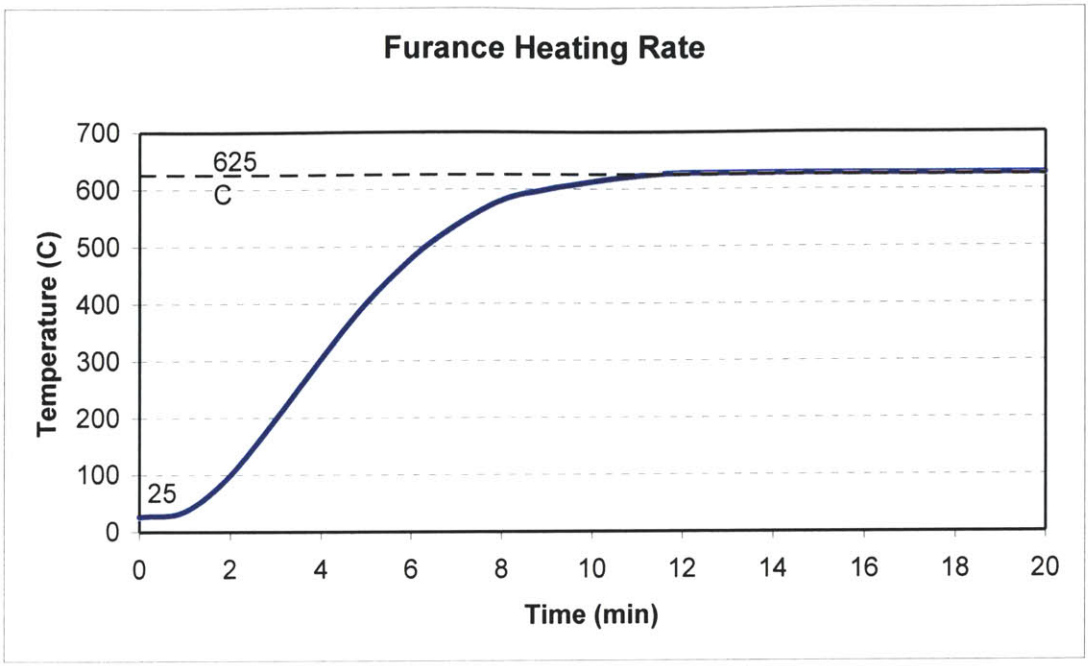

Figure 3.15 Furnace ramp up rate

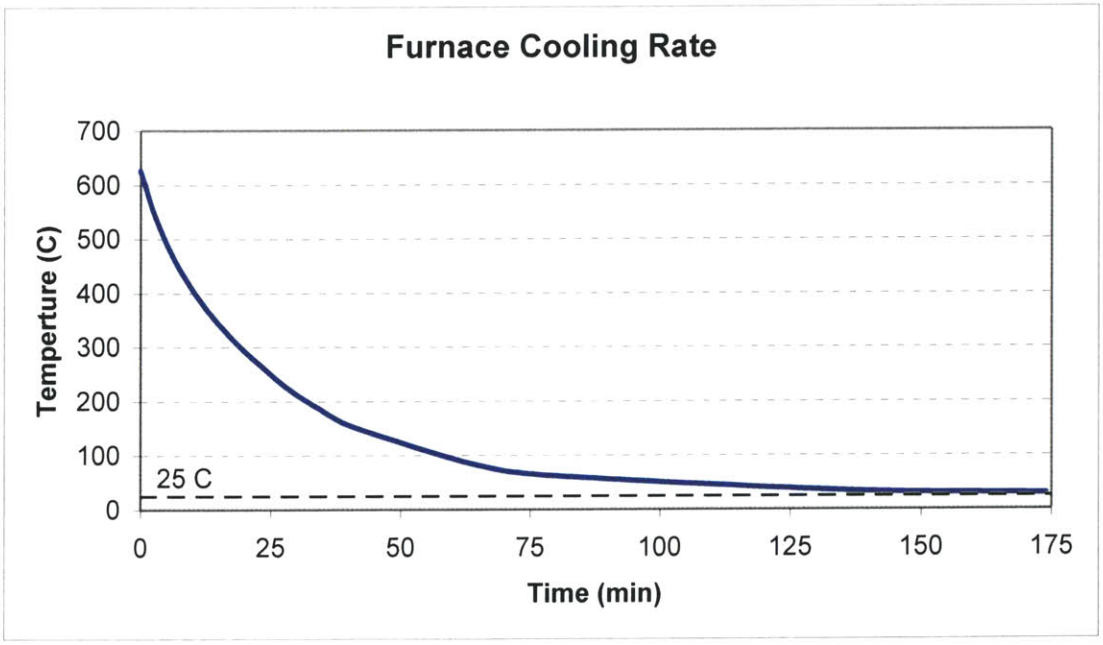

Figure 3.16 Cooling rate of furnace

Chapter 4. Infiltration Experiment

4.1 Experimental Setup

With the developed setup described in chapter 3, transient liquid-phase infiltration of aluminum was studied. All the infiltration experiments were conducted in the gold tube furnace with the aluminum gettering system.

4.1.1 Experimental Conditions

Table 4.1 shows the typical experimental conditions used for TLI experiments.

Table 4.1 Experimental Conditions for TLI

Furnace Atmosphere	N_2
Flow Rate	2 cfh
Furnace Pressure	5-8 inches of H_2O
Infiltration Temp.	600-625 ^{o}C
Dew Point	<< - 40 ^{o}C

The heating cycle of the furnace is controlled by using an Omega CN3251 controller. Figure 4.1 shows the typical heating cycle used for the experiments. The furnace is first purged with nitrogen for one hour to flush out the air before the temperature is ramped up. A fast ramp up and ramp down rate is used to minimize the duration for which the sample stays at a high temperature and to avoid oxidation at intermediate temperatures. The temperature and duration of the hold at steady state high temperature is based on the process requirements. Typically, a hold of 30 minutes at high temperature was used for infiltration experiments.

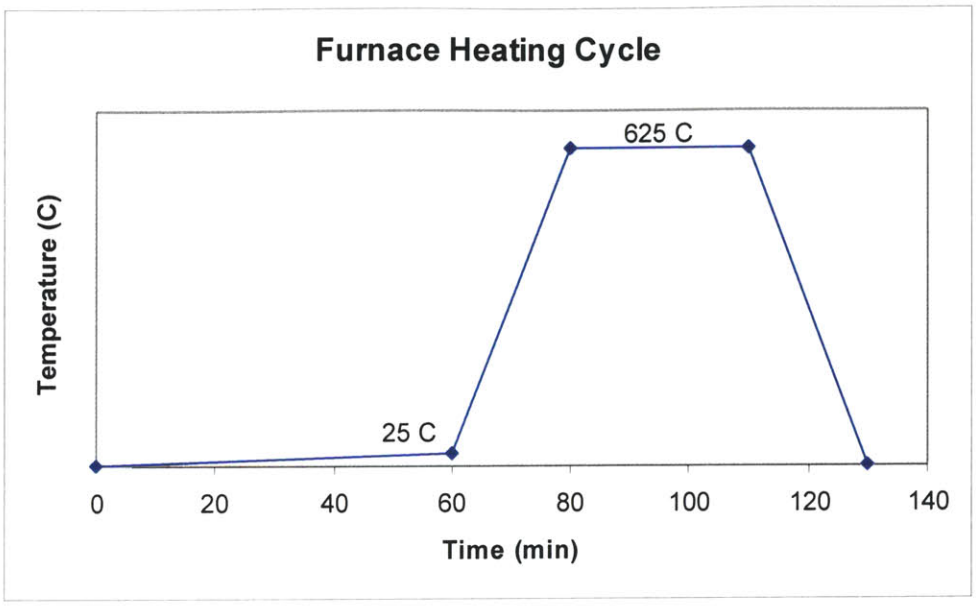

Figure 4.1 Typical Furnace Cycle

4.1.2 Powder Preform

In actual process, green parts of desired shape and complexity will be made from aluminum powder by SFF processes like 3DP. But in the current work, powder preforms were made by lightly pressing aluminum powder into simple shapes like circular discs or rectangular blocks. Pure aluminum powder is manually pressed into a circular disc in an Arbor Press and the shapes are made by filing. The packing density of these preforms is 64-65 % and has just enough strength to hold the powder particles together. Figure 4.2 shows a pressed aluminum disc. All the powder preforms were made from – 40 + 100 mesh (150 - 420 microns) aluminum powder.

Figure 4.2 Aluminum Powder Preform

4.1.3 Infiltrant

In most of the experiments 4047-Al was used as infiltrant. In some later experiments custom infiltrant were made using this as a precursor. 4047-Al is a standard aluminum brazing alloy (BAlSi-4) containing 11-13 % Si. Table 4.2 shows its nominal composition. Its solidus is 577 ^{o}C (1170 ^{o}F) and liquidus is 582 ^{o}C (1180 ^{o}F), as specified by the manufacturer and mentioned in the handbooks.

Table 4.2 Nominal Composition of 4047-Al

Element	Weight Percentage	Element	Weight Percentage
Aluminum	BALANCE	Copper	0.30 % max.
Silicon	11-13 %	Iron	0.8 % max
Magnesium	0.10 % max.	Zinc	0.20 % max.
Manganese	0.15 % max.	Beryllium	0.0008 % max.
Others	Each 0.05 % max.	Total	0.15 % max.

4047 Al was obtained in rod form from Eagle Alloy Corporation. It was first melted in the desired shape and quantity in the gold tube furnace and turned on a lathe to remove the hard oxide skin formed during solidification, before conducting infiltration experiments.

4.1.4 Experiments

Infiltration experiments were first conducted by simply putting the infiltrant on top of the powder preform. After the success of these experiments (Figure 3.10) gated infiltration experiments were conducted by the aluminum skeleton into the infiltrant melt only after the infiltration temperature was achieved. But liquid metal didn't infiltrate parts. On observing closely it was found that the surface of the infiltrant melt was covered with a thick oxide skin, and this prevented liquid metal from coming in contact with the skeleton. So, it was necessary to get rid of oxide skin of the melt to achieve infiltration.

4.2 Removal of Oxide from Surface of melt

As discussed above, one of the challenges for TLI in aluminum is strong oxide skin at the surface of the infiltrant melt. Because of high reactivity of aluminum, a strong, stable oxide film always encapsulates the infiltrant and this needs to be broken for infiltration.

This could be achieved by mechanically or chemically breaking the oxide skin. Chemical means of breaking the oxide would require using fluxes. Potential fluxes would be the ones used in aluminum brazing. But the problem with working with fluxes is that during infiltration there is a high probability that the flux will also get into the skeleton along with the liquid metal, contaminating the sample. So, chemical means was not pursued in detail.

Mechanical means were explored in detail and different methods to break the oxide skin were attempted. Techniques like using gravity to break the oxide skin or mechanically scrapping it from the surface of melt were tried out. Liquid melt was poured from a height of few centimeters to break the skin at the surface of the melt while pouring. But it didn't help in breaking the oxide skin, mainly because oxide skin was very strong and there was not enough gravitational head in the small furnace.

Next, the removal of the oxide skin was tried by mechanically scrapping it from top of the melt. A skimmer was made out of a machinable ceramic. It was dipped inside the melt from the top and rotated externally to scrape out the oxide. But the oxide skin was so strong that the skimmer couldn't penetrate through it. While rotating, liquid melt just kept getting displaced around the skimmer inside the oxide skin, never breaking out of it as if enclosed in a bag. Applying some downward external force also didn't help it.

Figure 4.3 Ceramic foam filter

Finally, ceramic foam filters were used to filter out liquid melt from the oxide. Ceramic foam filters were made by machining discs of ceramic foams of size close to crucible diameter and attaching it at the end of ceramic rod. The filter was pushed into the liquid melt from the top. The idea was to push the oxide skin to the bottom so that liquid metal filters out through pores. It worked successfully and helped to get clean liquid melt of infiltrant, which can be used for infiltration. Figure 4.3 shows the ceramic foam filter used for breaking the oxide skin on the infiltrant melt. Foam having 7-10 pores per inches (PPI) was used. These foams are commonly used for metal filtration. Usually silicon carbide ceramic foams are recommended for filtration of aluminum.

The schematic of the complete dipping mechanism is shown in Figure 4.4. For gated infiltration, the foam filter is first pushed from the top and the aluminum preform is then dipped immediately as clean liquid comes out.

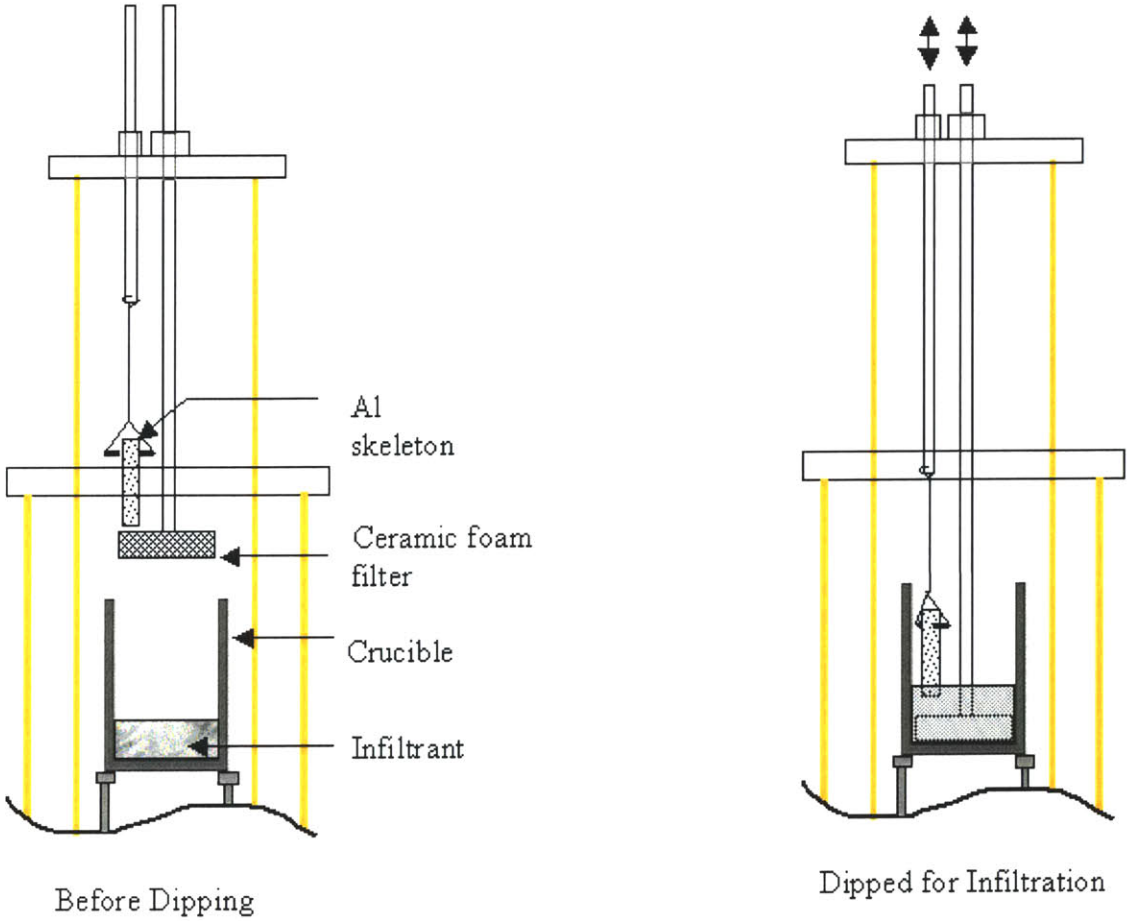

Figure 4.4 Dipping mechanism for gated infiltration

4.3 Breaking the Oxide on Aluminum Skeleton

Using ceramic foam filters helped in getting clean liquid melt of the infiltrant. But having clean melt in itself is not enough to facilitate infiltration in an aluminum skeleton. The presence of dense, stable oxide layer on the surface aluminum powder prevents infiltration, as the liquid metal doesn't wet its oxide. The contact angle has been reported to be 103° at 900 °C [25]. Therefore, it is necessary to reduce or break the oxide on the skeleton to enable effective infiltration. A few different methods were tried to get around the problem.

4.3.1 Coated Aluminum Powders

One of the most appealing ideas was to coat the aluminum powder with a thin layer of a relatively inert element so that there is no oxide on the surface to start with. Selection of such an element is very critical as it will stay in the part even after infiltration and will become part of the final composition, affecting final properties. So, it should be decided very carefully. The element should be relatively inert and should not be an undesirable element in aluminum alloys. Aluminum melt should wet it properly. The diffusivity of the element in aluminum should be such that it stays on the skeleton during processing and doesn't diffuse out prematurely. Lastly and most importantly, it can be coated easily on aluminum powder.

After careful consideration of diffusivity, values of different elements in aluminum at 600°C Iron, Copper, Nickel, and Silver were found to be good candidates for coating material. These elements have relatively low diffusivity values in aluminum in that order. Table 4.3 shows the diffusivity value and characteristic diffusion length (for T = 100s, typical infiltration time) for trace amounts of these elements in aluminum (source [30]).

Table 4.3 Diffusivity (D) of Elements in Aluminum

Element	A1 (cm^2/s)	Q1 (KJ/mol)	T (K)	D (cm^2/s)	Diffusion Length ($\sqrt{4DT}$, microns)
Fe	135	192.6	875	4.3×10^{-10}	41.4
Cu	0.647	135.1	875	5.6×10^{-09}	149.2
Ni	4.4	145.8	875	8.7×10^{-09}	186.5
Ag	0.13	117.2	875	1.3×10^{-08}	228.9

4.3.2 Silver Coated Aluminum Powder

Even though silver has relatively high diffusivity as compared to other selected elements, it was attempted first primarily because it is easy to coat on aluminum powder and is readily available. Addition of silver in aluminum alloy improves its strength and is used in some premium-strength alloys. It contributes to precipitation hardening and stress-corrosion resistance.

Aluminum is coated with silver by the Electroless plating process. Silver coated aluminum powder of – 200 mesh (< 75 microns) size was obtained from Alfa Aesar. It contained 19-21-wt% of silver. Figure 4.5 shows the SEM photograph of silver coated aluminum powder and a close up of its coating. Coating thickness is of the order of 0.1-0.3 microns.

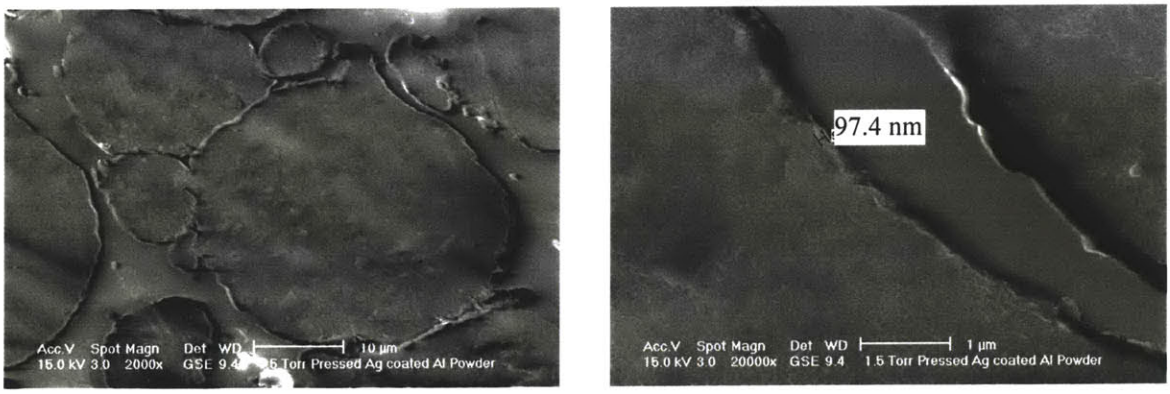

Figure 4.5 Silver coated aluminum powder

The wetting of liquid infiltrant (4047 Al) on silver was tested by putting it on silver foil under desired experimental conditions i.e. at 625 °C under nitrogen atmosphere. It spread nicely onto the foil leaving an oxide skin on the top (Figure 4.6). This implies that infiltrant nicely wets silver.

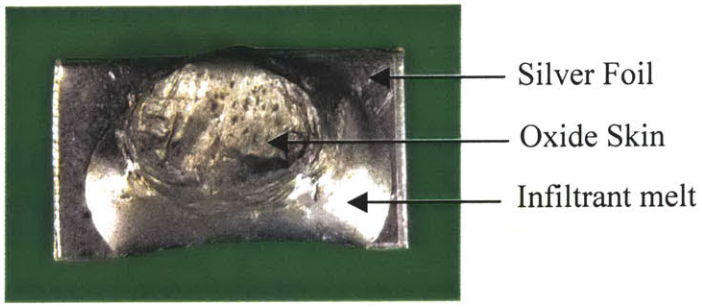

Figure 4.6 Wetting experiment on silver foil

Experiments were then conducted to infiltrate silver coated aluminum powder. Pressed powder samples were kept in the furnace at 625 °C with infiltrant on the top. The sample got sintered a bit but infiltrant didn't get into the skeleton. Gated infiltration was tried next but it also failed. Figure 4.7 shows the result of infiltration experiment and microphotograph of the sample. As it can be seen from the micrograph, silver coating failed during the process as it quickly diffused into the powder.

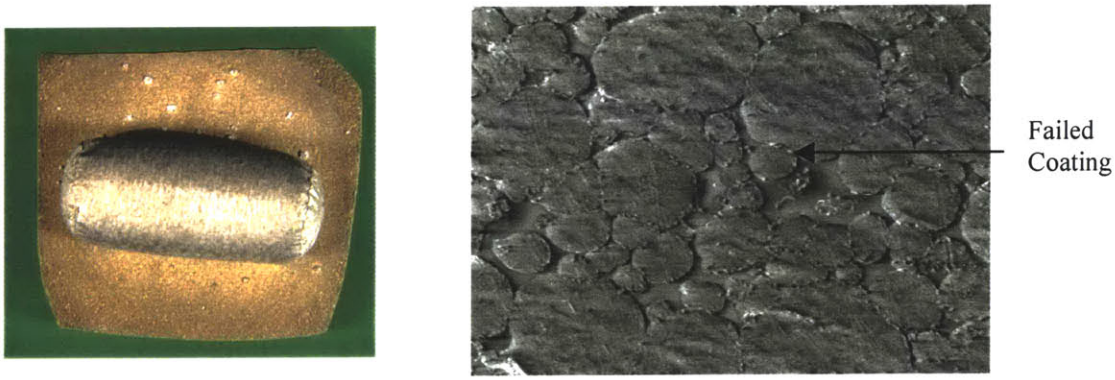

Figure 4.7 No infiltration of silver coated aluminum part

One possibility was to use a thicker coating on the aluminum powder and try it again to see if parts infiltrate. But before that, experiments were conducted with pure silver powder to check the infiltration depth. These experiments revealed that aluminum infiltrant melt doesn't infiltrate even pure silver powder. It freezes prematurely. Infiltration depth was observed to be only a few millimeters. Figure 4.8 shows the result of infiltration experiment and the micrograph of partially infiltrated silver part. Microprobe analysis of these samples showed that aluminum diffused into the silver powder even in the un-infiltrated portion and infiltrated part got homogenized implying very high inter-diffusivity and solubility. The diffusivity of Ag in Al is 1.3×10^{-8} cm^2/s

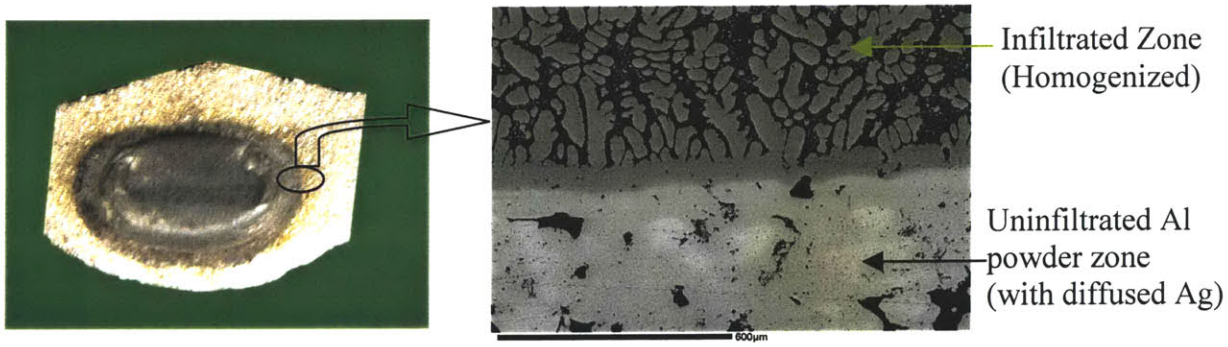

Figure 4.8 Infiltration of pure silver powder part

and its solid solubility is 55.6-wt%. Thus, there was a little hope of success with silver coated powder even with thicker coating and it was not explored further.

4.3.3 Metallic Coating on Aluminum Powder

To test the feasibility of other metal coatings on aluminum powder, custom made iron, copper and nickel coated aluminum powders were obtained from Powdermet Inc. The powder size was – 40 +100 mesh (150-420 microns), same as that of pure aluminum powder used in the experiments and a coating thickness of 1 micron was sought. These metallic coating on aluminum powder were done by vapor plating using patented Fluidized Bed Chemical Vapor Deposition processing technology (FBCVD) [22]. In the FBCVD process, powder particulates are injected at high concentration into a high velocity fluidizing gas stream, where they are fluidized in the turbulent fluidization regime. Through operation in the turbulent fluidization regime, powders can be uniformly handled with minimal agglomeration and particles are kept separated during coating. Once fluidized, the particles are heated and an organometallic precursor is added. The organometallic precursor, typically a carbonyl or metal alkyl, is decomposed to form the desired coating and organic byproduct, which is subsequently removed from the system. Normally a Slow Bed reactor is used for powder sizes larger than 20 microns. For these coatings, a lab scale Slow Fluidized Bed reactor was used and is schematically shown in Figure 4.9.

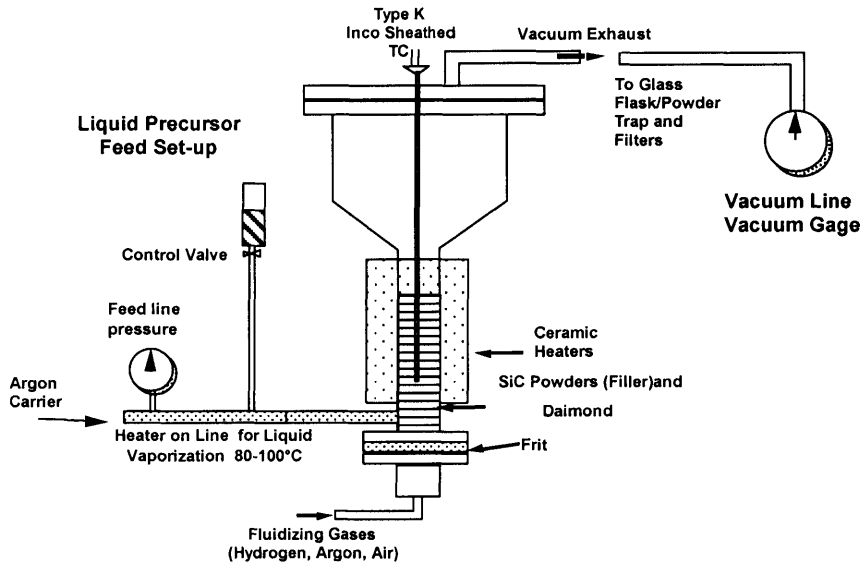

Figure 4.9 CVD Fluidized bed reactor

A summary of run conditions for each element is shown in Table 4.4

Table 4.4 Run conditions for metallic coating on aluminum powder

Run	Precursor	Gas Flow (SSCM)	Temp (°C)	Vacuum (in Hg)	Wt %
1	Ni Carbonyl	900 H2 300 Ar	140-160	-20 to 24	13.2 % Ni
2	Fe Carbonyl	900 H2 300 Ar	180-220	-20 to 24	9.2 % Fe
3	Cu Formate	900 H2 300 Ar	350-400	-20 to 24	11 % Cu

The expected coating thickness and volume percentage of coating is given in Table 4.5 assuming spherical aluminum powder particles of diameter 150 microns.

Table 4.5 Expected coating thickness and volume percentage of coating material

Coating	Wt %	Thickness	Volume %
Fe	9.2%	0.9 micron	3.1 %
Ni	13.2%	1.2 micron	4.6 %
Cu	11%	1 micron	3.8 %

4.3.4 Iron Coated Aluminum Powder

Iron coated aluminum powder is a good candidate for infiltration experiments as diffusivity of iron in aluminum is low (4.3×10^{-10} cm^2/s). The solubility of iron in aluminum is also very low (~ 0.05-wt%). This means iron will not diffuse inside the powder and the coating will fail only by dissolution in liquid infiltrant and would always stay in the infiltrated region only. Though iron is not a very common alloying element in aluminum, it is sometimes added to increase hot tear resistance of the alloy. Iron reacts to form a myriad of insoluble phases in aluminum alloy melts like $FeAl_3$ and $\alpha AlFeSi$.

These essentially insoluble phases are responsible for improvements in strength especially at elevated temperatures.

The coated powders have approximately 9.2-wt% iron and coating thickness is of the order of 1 micron. Figure 4.10 shows an SEM photograph of iron coated aluminum powder and a close up of its coating.

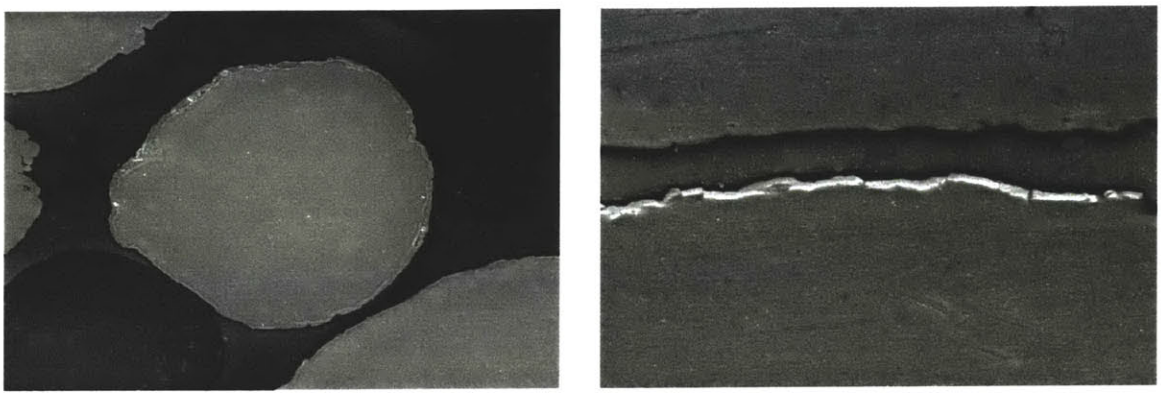

Figure 4.10 Iron coated aluminum powder

The wetting of liquid infiltrant on iron was again tested by putting it on an iron plate under desired experimental conditions i.e. at 625 ^{o}C under nitrogen atmosphere. But it didn't spread nicely as in the case of silver powder (Figure 4.11). This could not necessarily mean non-wetting because of the presence of oxide skin on the surface of infiltrant. Oxide could prevent nice spreading of infiltrant even if it wets the surface.

Figure 4.11 Wetting of infiltrant on iron

So gated infiltration experiments were directly conducted with coated aluminum powder where there is no problem of oxide skin. With the dipping mechanism, oxide skin on infiltrant was broken prior to infiltration. Powder preforms were made by pressing the powder in an arbor press and gated infiltration was conducted by dipping it in infiltrant

melt at 625 °C for 10 minutes. Figure 4.12 shows how parts look before and after infiltration experiments (figures doesn't show same part). There was no infiltration at all. Infiltrant didn't wet the coated powder sample.

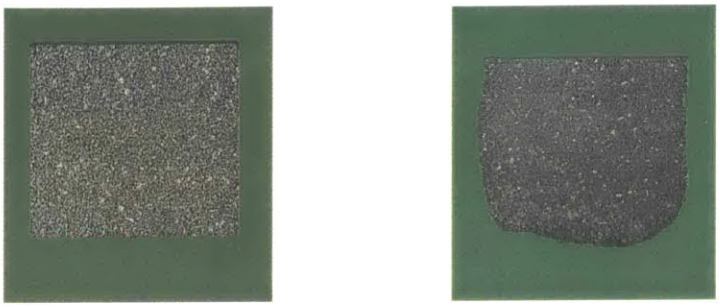

Before Infiltration After Infiltration

Figure 4.12 Gated infiltration of iron coated aluminum powder

Gated infiltration of iron powder (1018 steel, containing 99% iron with 0.2% C and 0.8% Mn) preform with this infiltrant confirmed that the problem was indeed wetting. Infiltrant didn't wet this powder which contains mainly iron (Figure 4.13).

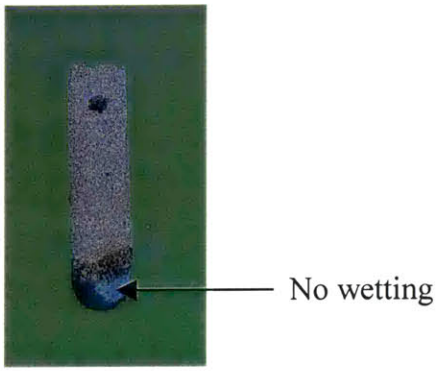

Figure 4.13 Infiltration experiment with iron

4.3.5 Copper Coated Aluminum Powder

Copper coated aluminum powder is another candidate for infiltration experiments. The diffusivity of copper in aluminum is 5.6 x 10^{-09} cm^2/s. The copper coated aluminum powder had 11-wt% Cu and coating thickness was of the order of one micron. Figure 4.14 shows a SEM photograph of copper coated aluminum powder and close-up of its coating.

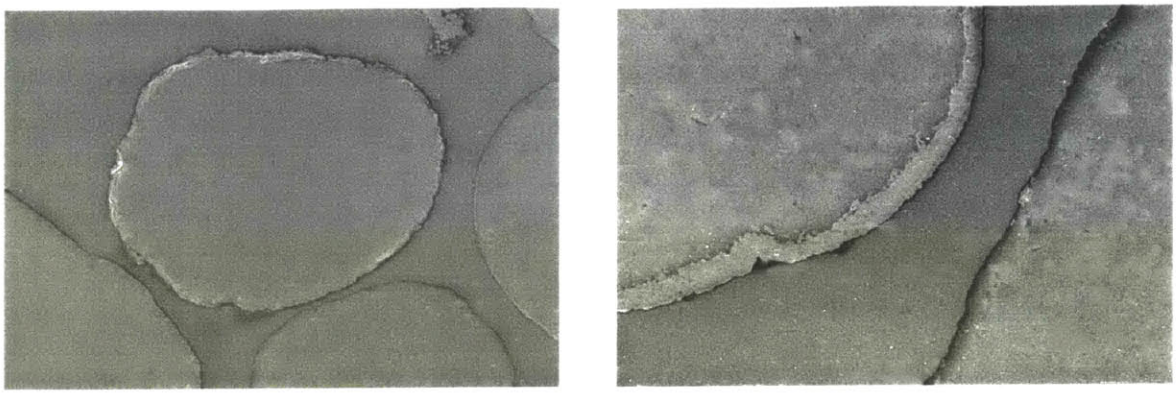

Figure 4.14 Copper coated aluminum powder

Gated infiltration experiments were conducted with powder preforms made of this powder and dipping it in infiltrant at 625 °C for 10 minutes. Figure 4.15 shows how the parts look before and after infiltration experiments (figures doesn't show same part).

Before Infiltration After Infiltration

Figure 4.15 Infiltration experiment with copper coated aluminum powder samples

As seen from the change in color, all the copper diffused out into the powder part but there was no infiltration. In a separate run when the powder preform was kept at 625 °C for just 5 min and cooled down without introducing infiltrant, all the copper was still gone. This indicates that copper is diffusing into the powder prematurely. This is not unexpected as solubility of copper in aluminum is quite high (5.67-wt% solid solubility and 33.15-wt% liquid solubility). SEM photographs confirms this premature coating failure. All the coatings were gone and aluminum copper eutectic was observed inside the powder particles (Figure 4.16). This was formed because copper diffused into the aluminum and local melting would have occurred where composition was near eutectic composition. The Al-Cu eutectic melting point is 546 °C.

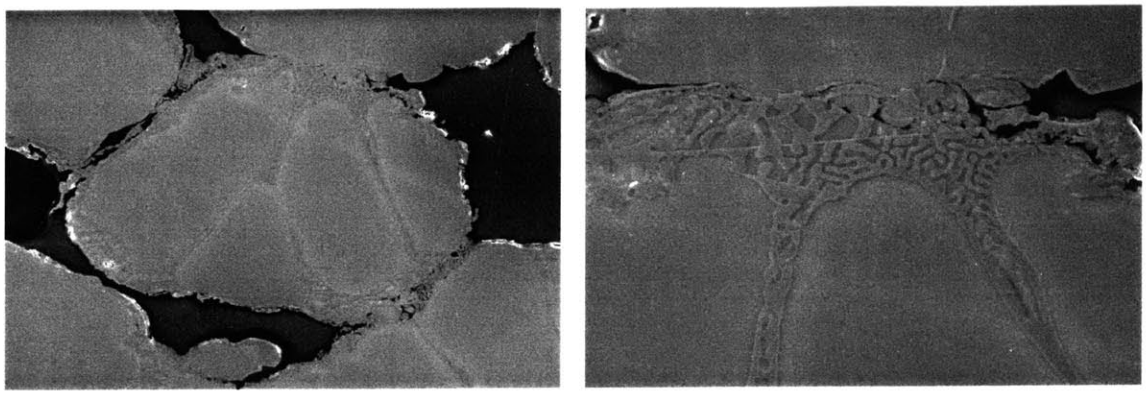

Figure 4.16 SEM photograph of infiltrated copper coated Al sample

4.3.6 Nickel Coated Aluminum Powder

Nickel coated aluminum powder was tried next. Figure 4.17 shows the SEM photograph of nickel coated aluminum powder. The coating thickness was of the order of one micron.

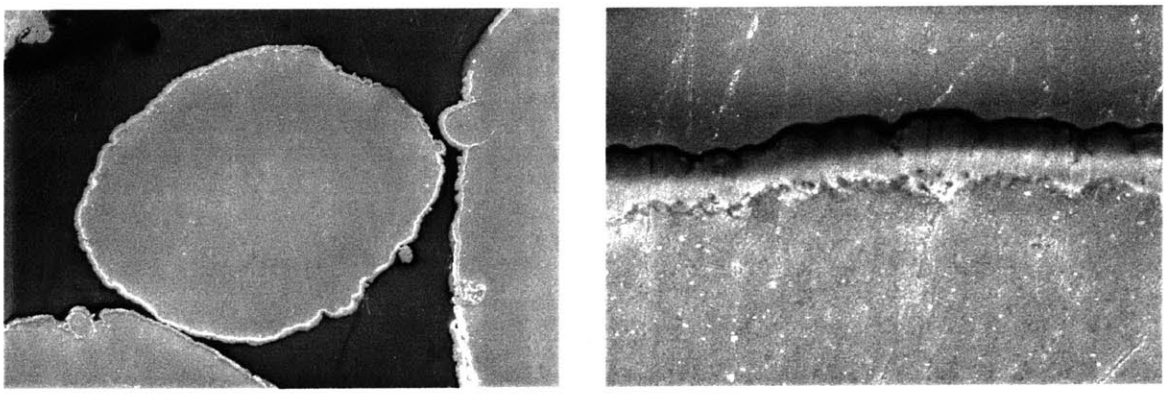

Figure 4.17 Nickel coated aluminum powder

In general, nickel is added to aluminum alloys to improve hardness and strength at elevated temperatures and to reduce the coefficient of thermal expansion. The nickel aluminum system is known to be a reactive infiltration system [19]. They are used to form nickel aluminides, which are ordered intermetallic compounds (Ni_3Al and NiAl), and are used in high-temperature structural material. The infiltration is accompanied by an exothermic reaction. Therefore, experiments were done carefully with nickel coated aluminum powder. Powder preforms were dipped in liquid infiltrant at 625 ^{o}C for 10 minutes. But no infiltration was achieved in this case also. Figure 4.18 shows how parts look before and after infiltration (figures doesn't show same part).

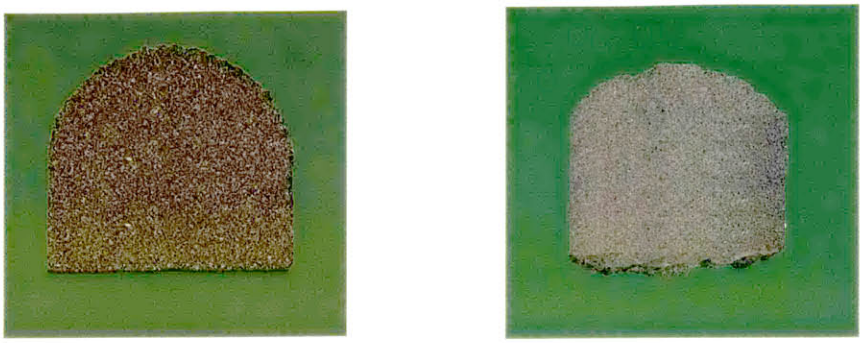

Before Infiltration After Infiltration

Figure 4.18 Infiltration experiment with nickel coated Al powder sample

4.4 Improving Wetting behavior of Infiltrant

Another idea was to use a wetting agent in the infiltrant to improve it's wetting with aluminum powder and to cause infiltration. Magnesium is a commonly used wetting agent in flux-less aluminum brazing. Trace additions of a highly reactive element like magnesium in the melt enhances wetting by breaking the oxide layer as the reactive element will preferentially react with oxygen and will reduce the aluminum oxide. Once the oxide layer is broken, the melt can diffuse through the cracks, lift the oxide layer and will allow metal-metal contact to occur, facilitating infiltration.

4.4.1 Custom Infiltrant

Custom infiltrant was made by adding magnesium to existing aluminum-silicon alloy (4047 Al). Usually it is very difficult to add pure magnesium in molten aluminum as it is lighter than aluminum and starts floating on the melt. This causes drossage of magnesium by oxidation and burn-off and it would be hard to control the exact composition of the melt. So, magnesium was added in the infiltrant using Al- Mg master alloy. These master alloys contain magnesium in solution form with aluminum and are much easier to work with 68 % Mg-Al master alloy was obtained from KB alloys in button form. Because the density of 68 % Mg-Al is greater than that of pure magnesium (2.0 g/cc as compared to 1.7 g/cc), it has fewer tendencies to float and burn off. Less burn-off means fewer oxides, better recoveries and cleaner melts. With its low melting point (473 ^{o}C), the 68 % Mg-Al alloy melts before it can resurface and burn-off.

The melt treatment process is simple and was done by putting chunks of master alloy together with 4047 Al rod pieces in a graphite crucible and melting them at 625 °C for 30 minutes. Oxide layer encapsulating the rod pieces were broken by plunging ceramic foam filter to ensure better mixing of the alloys. An inert atmosphere was used to minimize oxidation of the melt. The alloys were mixed by weight to get the required composition.

4.4.2 Infiltration

A target composition of 10-wt% of Mg was tried. Experiments were conducted with this infiltrant at 625 °C under high purity nitrogen atmosphere. The custom infiltrant made by melting was cleaned by turning it on a Lathe to remove the hard oxide formed during solidification. Gated infiltration was carried out by first breaking the oxide layer on infiltrant melt surface using the ceramic foam filter and then dipping the pure aluminum skeleton in the clean melt for 30 min. The infiltrant filled one-inch sample up to the top. Figure 4.19 shows the infiltrated part.

Figure 4.19 Infiltrated part

4.4.3 Reducing Magnesium Content

The infiltrant used for successful infiltration had 10-wt% Si and 10-wt% Mg. Assuming a initial packing fraction of 0.6 for the skeleton, the final composition of the infiltrated sample will be 4.6 wt% Si and 4 wt% Mg. This magnesium content is quite high as compared with any commercially available aluminum alloy containing both Si and Mg. So, attempts were made to reduce the magnesium concentration of the final part by reducing its amount in the infiltrant. Moreover as seen in the phase diagram (Figure 4.20) for a mixture of 12% Si-Al and 68% Mg-Al alloys (representative of infiltrant) 10% Mg

is on the right side of eutectic composition. During infiltration, the final composition of the infiltrated part will move towards a more liquid state.

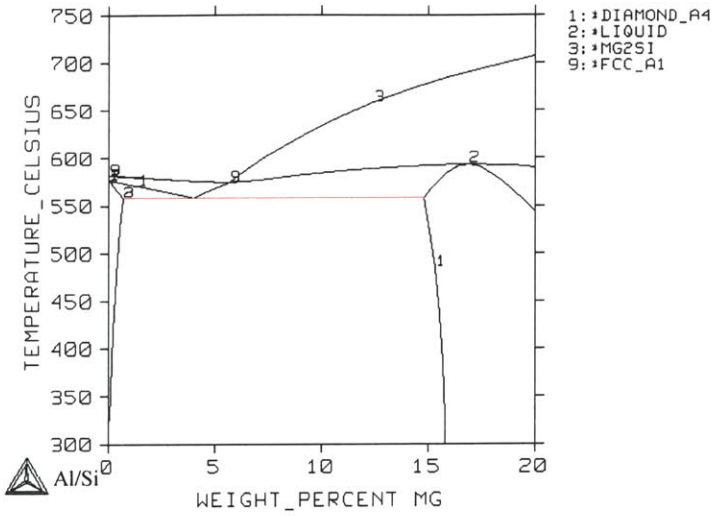

Figure 4.20 Phase diagram of mixture of 4047 Al and 68%Mg-Al alloy

So, magnesium concentrations near or in the left of eutectic point were selected for the infiltrant. Composition of 4-wt% Mg and 2-wt% Mg in the infiltrant were tried. In both the cases, 1" tall samples were infiltrated up to the top in gated infiltration.

Chapter 5. Characterization of Infiltrated Part

5.1 Role of Magnesium in TLI

As mentioned in the last chapter, additions of magnesium in the infiltrant caused a dramatic difference in the infiltration response of the aluminum system. The oxide layer present on the powder particles prevents wetting and therefore infiltration by capillary action. When Mg is added in the infiltrant, infiltrant wets the powder skeleton facilitating infiltration. The infiltration rate is though very slow. In a typical wetting system, 1" powder skeleton of the given powder size should get infiltrated within a minute. However, an infiltration time of 30 min. was required for the aluminum TLI experiments. No infiltration was observed during initial few minutes followed by a very slow infiltration, implying that some kind of reaction was facilitating the infiltration.

Magnesium is highly reactive, and the free energy of formation of its oxide is more negative than that of the oxides of aluminum. Magnesium, therefore, has the potential to act as a reducing agent in this system. This suggests that the magnesium could reduce the aluminum oxide, rupturing the oxide skin sufficiently to facilitate diffusion, wetting, and infiltration. A possible reaction is:

$$3Mg + 4Al_2O_3 \rightarrow 3MgAl_2O_4 + 2Al \qquad [5.1]$$

which is a partial reduction to form cubic spinel and aluminum. The complete reduction of alumina to MgO has been shown to become dominant in alumina based metal-matrix composites at Mg concentration between 2 and 4% [29]. In this case reduction reaction is:

$$3Mg + 2Al_2O_3 \rightarrow 3MgO + 2\,Al \qquad [5.2]$$

A possible mechanism for infiltration of aluminum powder due to addition of Mg in the infiltrant could be that magnesium in the melt enhances wetting by breaking the oxide layer. Where aluminum powder is in contact with the infiltrant, the magnesium in the infiltrant preferentially reacts with oxygen and reduces the aluminum oxide. Once the aluminum oxide is broken, the melt can diffuse through the cracks, lift the oxide layer,

and allow metal-metal contact to occur, facilitating infiltration. The nearby aluminum particles that were not directly in contact with infiltrant are subsequently exposed to the infiltrant and their oxide layers are disrupted. Since infiltration proceeds by gradual disruption of oxide skin, it takes a longer time for infiltration to complete.

The beneficial role of Mg has also been reported in fluxless aluminum brazing [1] and liquid-phase sintering of aluminum alloys [9]. In the later, trace additions of magnesium dramatically improved the sintering response of the pressed aluminum. This was attributed to magnesium disrupting the passivating Al_2O_3 layer through the formation of a spinel phase. It was reported that 0.15% Mg is required to attain peak sintered density in pressed aluminum [9] and approximately 4% Mg is required for freeform-fabricated aluminum part [5]. In a patent literature [7], it has been reported that nitrogen atmosphere helps in reduction of oxide layer present on the Al powder particles. When magnesium is vaporized into a nitrogen atmosphere, it reacts to form magnesium nitride. It is then thought to reduce Al_2O_3 by:

$$2Mg_3N_2 + Al_2O_3 \rightarrow 2AlN + 6\ MgO + 2\ Al + N_2 \qquad [5.3]$$

The reaction between Mg and N_2 at high temperatures occurs only in the vapor state. Mg loss due to vaporization has been detected above 200 °C [28]. Therefore, this mechanism of oxide reduction is assumed predominant way, especially in freeform products where most of the porosity is open and reaction between oxide and Mg_3N_2 can occur throughout the specimen. To test it, infiltration experiments were conducted in pure Argon atmosphere at 600 °C with an infiltrant containing 4% Mg. Unlike the case reported in [5], parts infiltrated completely even in argon atmosphere. Therefore, it is believed that the above reaction (5.3) is not the predominant method of oxide reduction in the infiltration experiments.

5.2 Final Part Composition

The composition of final part is decided by initial powder composition, packing fraction of the green part, infiltrant composition and infiltration temperature. Infiltration temperature plays an important role in deciding the final composition, as the composition of the liquid that infiltrates the part is a strong function of the temperature. For a given

temperature, if the infiltrant composition lies in two-phase field, the temperature and not the infiltrant composition will decide the composition of the liquid. For example, in Al-Si binary system at 620 °C the liquid composition will always be 5.73% Si for all the infiltrant containing 0.84% to 5.73% Si. The composition of the infiltrant will only decide the percentage amount of liquid that will be there in the infiltrant at that temperature. However, if the infiltrant composition is not in the two-phase field the liquid composition will be same as the infiltrant composition.

In the TLI experiments, the powder preforms were made of pure aluminum powder. Its packing fraction is of the order of 60%, which is comparable to green part densities obtained by 3DP. So assuming an initial packing fraction of 0.6 for the skeleton, the final composition of the infiltrated part can easily be calculated from mass conservation. With an infiltrant containing 12% Si and 4% Mg the final average composition of the infiltrated part will be 4.4-wt% Si and 1.6-wt% Mg. This composition is similar to that of aluminum alloy DF95 listed on Matweb with little less copper. Similarly with infiltrant containing 12% Si and 2% Mg the final average composition of the infiltrated part will be 4.6% Si and 0.8% Mg. This composition is again very close to casting alloy Aluminum 355.0 with less copper. Therefore, by properly tailoring the infiltrant composition the composition of the final infiltrated part can easily be matched to commercially available aluminum alloys.

Figure 5.1 shows the ternary phase diagram of Al-Mg-Si at 600 °C. In the close up of the phase diagram (Figure 5.2) is marked the infiltrant composition (12% Si and 4%Mg) and resulting final part composition. The infiltrant is completely liquid at 600 °C. Therefore, composition of the liquid that infiltrates will be same as that of the infiltrant. The final part composition is in the two-phase region and will have 51.5% pure aluminum phase and 48.5% of liquid phase if diffusion of the elements is complete. The original solid content was 60%, pure aluminum powder. This means there will be some melting of the aluminum powder during the process. If too much of the liquid is formed then the green part may loose strength and will not be able to retain the original shape resulting into loss of accuracy. So, infiltration temperature and infiltrant composition should be selected with proper care.

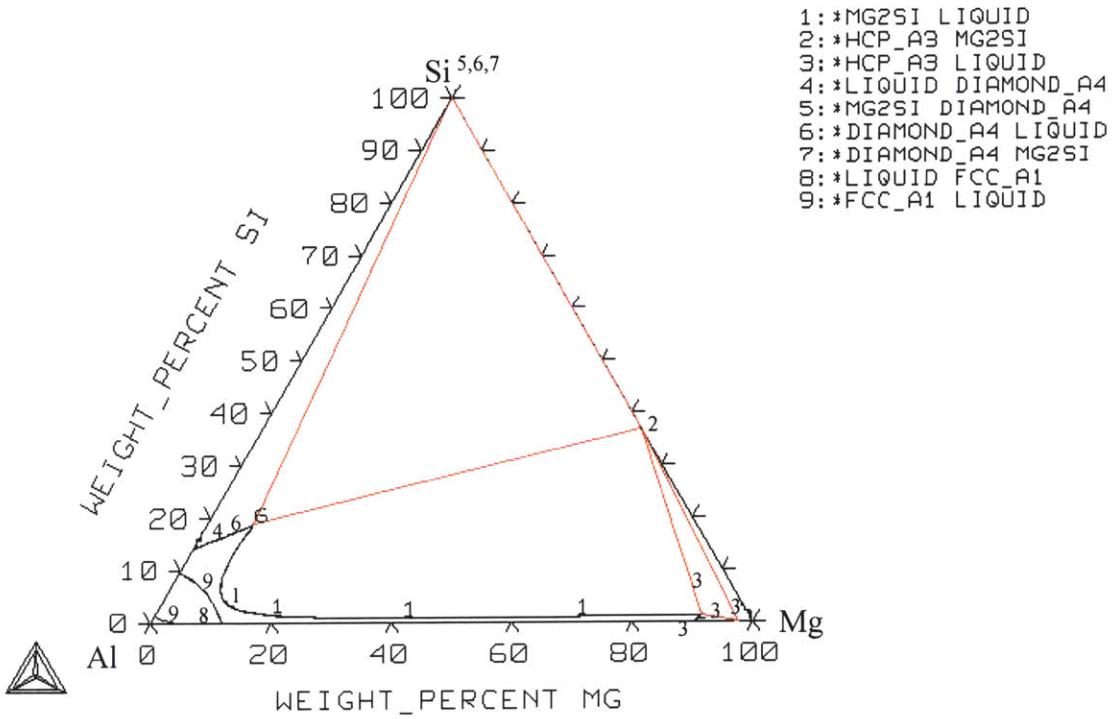

Figure 5.1 Ternary Phase diagram of Al-Mg-Si system at 600°C

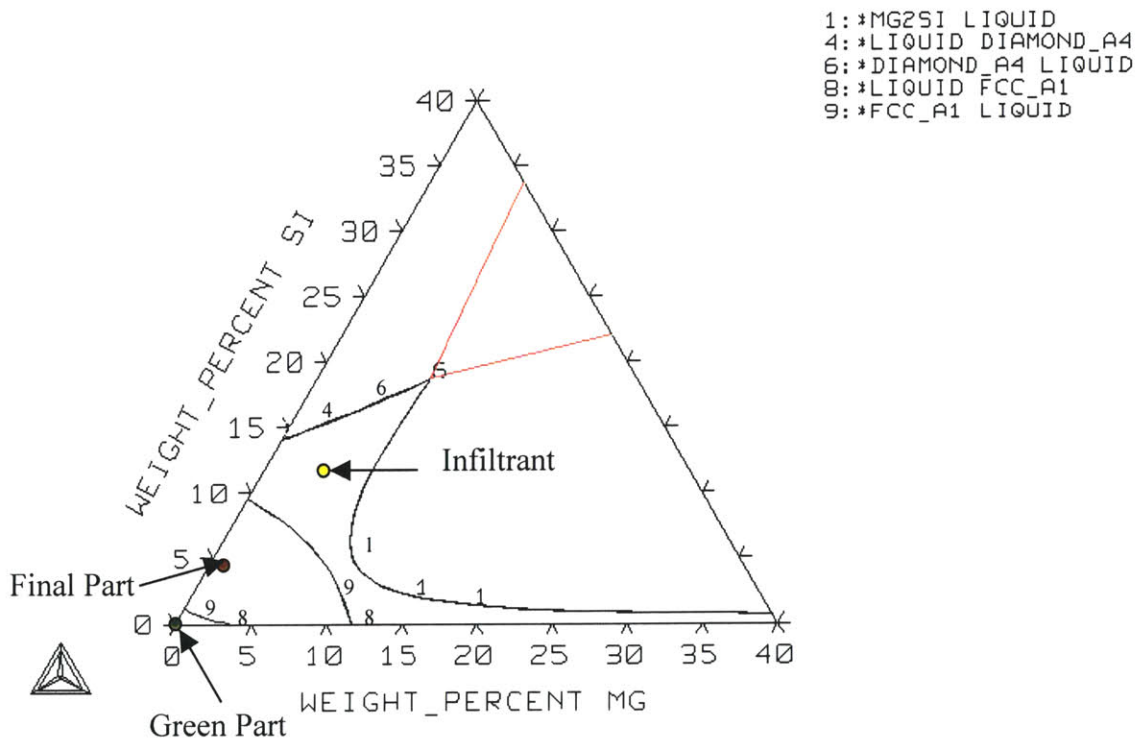

Figure 5.2 Ternary phase diagram with infiltrant, green part, and final part composition marked

Usually in a two-element system like Ni-Si, infiltrant is selected such that it is saturated with silicon or in other words sits on the liquidus, so that it doesn't dissolve base material from the skeleton that causes erosion of the sample. Similarly, in the ternary system like Al-Mg-Si, infiltrant composition can be selected on the liquidus to avoid any potential of erosion of the powder skeleton.

5.3 Microstructure Characterization

Infiltrated parts were studied microscopically for distribution of infiltrant in pores, formation of different phases, grain sizes and presence of residual porosity. Metallographic specimens of the infiltrated parts were prepared as per standard procedures for examination under the microscope. Since aluminum and its alloys are soft and easily scratched or distorted during preparation, so proper care should be taken in sample surface preparations like high wheel speed and large loads in automatic polisher should be avoided. Moreover, with the inherent porosity of most P/M materials it is essential in the surface preparation to remove all smeared metal and clearly identify the pores.

For microscopic analysis, infiltrated samples were vacuum impregnated with, and mounted in epoxy resin, to fill any residual porosity. Using a sample cup or holder to form the mount, a ¾ -in. deep layer of epoxy was poured over the sample in the cup. The cup was evacuated to 100 Torr and held at that pressure for 10 minutes. Ambient pressure was restored, forcing the resin into most of the sample. Curing was done at room temperature.

The cured mounts were ground at 120, 500, 1200 and 4000 mesh wet SiC paper, on a rotating wheel, with rotating direction changed 90^{o} after each paper. Usually polishing was done on automatic polishing wheel and a wheel speed of 150 rpm and load of 25 N was used. Final polishing was done with 0.3 micron deagglomerated alumina on napped cloth in automatic polisher. Since there was possibility of presence of reactive compound like Mg_2Si in the infiltrated part, many times waterless polishing was used in the final stages to avoid loss of reactive particle by corrosion. Diamond paste on nap cloth was used in these cases.

Prepared samples were examined under optical microscope and SEM to study the microstructure of the infiltrated part. Figure 5.3 shows the typical microstructure of the infiltrated part. Figure 5.4 shows higher magnification images.

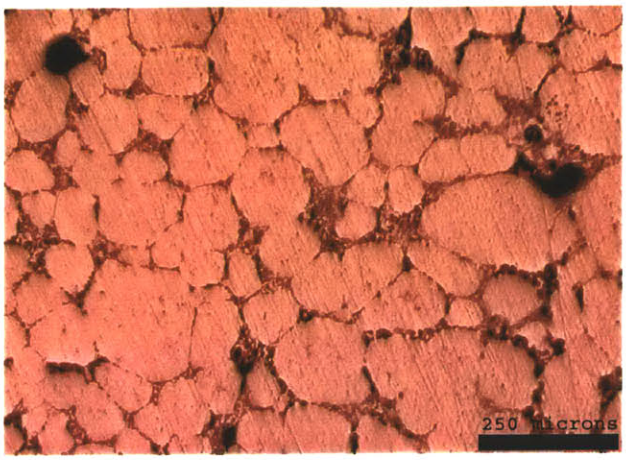

Figure 5.3 Microstructure of Infiltrated Part

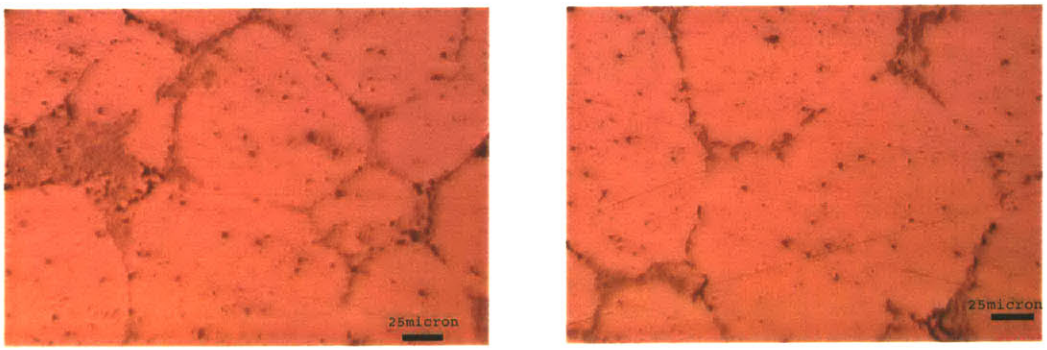

Figure 5.4 Microstructure of infiltrated area

As expected, the final microstructure is not a single-phase solid solution of the melting point depressant in the skeleton material due to lower solubility of silicon in aluminum. The original void space that was filled with liquid has a two-phase microstructure. This resembles that of a cast microstructure (Figure 5.5). The powder particles that have absorbed Si and Mg and have taken place of the primary dendrites those solidify first in a casting. The remaining infiltrant has a eutectic microstructure similar to the sections of a casting between the dendrites that are the last to freeze. Since this type of microstructure

is still desirable and widely accepted in industry, the fact that the material composition is not uniform throughout is not a drawback. Two-phase strengthening is common for commercial net-shape casting alloys.

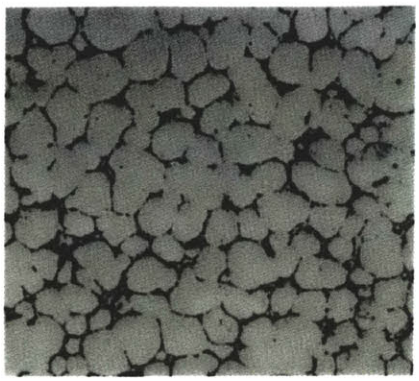

Figure 5.5 Die cast microstructure of 443-F Al containing 4.5-6% Si [1]

Only drawback of the infiltrated part is that it has a lot of residual porosity. Although residual porosity is not uncommon in powder metallurgy parts but its high percentage in final infiltrated part might not be acceptable for many application.

Microprobe analysis was done on the part infiltrated with the infiltrant containing 4-wt% Mg and its result is shown in Figure 5.6. The values shown are average of five sample points in each region. Some of the silicon and magnesium diffused into the powder but most of it is still in the two-phase region surrounding powder particles.

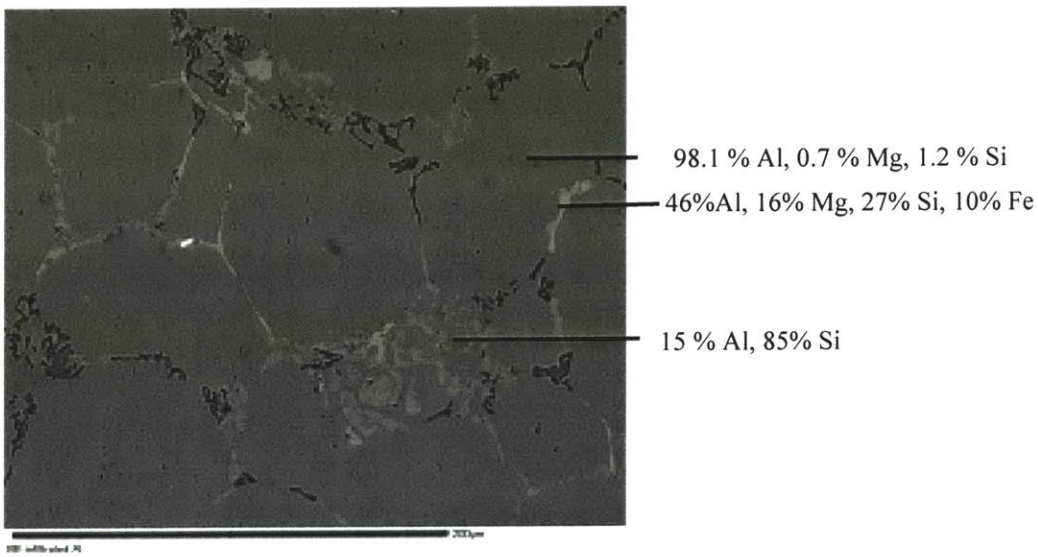

Figure 5.6 Composition analysis of infiltrated part

5.4 Infiltrated Part Density

Since microstructure analysis revealed the presence of some residual porosity, Archimedes test was done on the infiltrated part to determine its apparent density and porosity levels. The actual density of fully dense aluminum part with 4.4-wt% Si and 1.6-wt% Mg should be 2.66 g/cc. This was calculated based on densities of individual phases that would be present in the part and their relative amounts if it were in the equilibrium. For the parts with above-mentioned composition, thermocalc analysis shows that it should have 94-wt% Al, 3.5-wt% Si and 2.5-wt% Mg_2Si at room temperature. So based on mass conservation the final density of this material should be 2.66 g/cc. Same result was obtained when theoretical density was calculated using elemental densities and their weight percentage in the sample. These calculations give only approximate value of the theoretical density as the final part has different microstructure than that predicted by the phases in thermocalc. A more accurate determination of the theoretical density can be done by determining the density of the powder particles, with diffused Si and Mg based on their solubility limits, and different phases present in the infiltrated zone and their relative amounts determined theoretically. However, the result doesn't vary much.

For measuring apparent density, parts were first cleaned and its dry weight (W_1) was measured. The volume of the infiltrated part was then determined by Archimedes test. In order to accurately determine the volume of the test piece by water displacement, the samples were impregnated with wax to close all the open pores. Care was taken to remove all the excessive wax from the surface. The weight (W_2) of the waxed sample was measured. The wax impregnated test piece was then suspended in deionized water using a fine wire so that sample was completely submerged and only wire breaks the water surface. All the air bubbles were removed and submerged weight (W_3) of the sample was measured. Figure 5.7 shows the setup that was used for weight measurements. The balance was re-zeroed before every measurement so that different weights of only sample were measured without any external error.

The volume of the sample (V) was then determined using Archimedes principle,

$$\rho_w V = W_2 - W_3 \qquad [5.4]$$

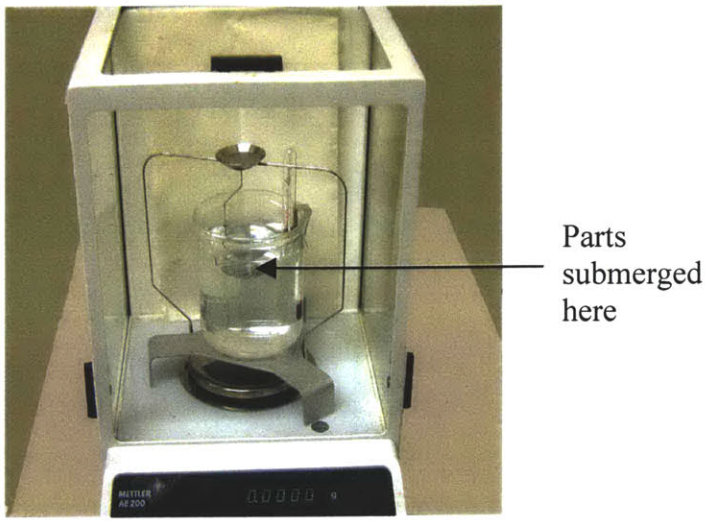

Figure 5.7 Archimedes test setup

And apparent density, ρ_{app} (in %) of the part was calculated using the following formula

$$\rho_{app} = \frac{W_1}{W_2 - W_3}\frac{\rho_w}{\rho_a} \qquad [5.5]$$

where ρ_a is theoretical actual density of material and ρ_w is density of water. ρ_w is approximately equal to 1 at room temperature.

The density of parts, infiltrated at 600 °C with an infiltrant containing 4-wt% Mg and 11-13wt% Si, measured this way was of the order of ~ 2.4 g/cc i.e. parts were 90-91% dense. Similar results were obtained for the parts infiltrated with an infiltrant containing 2-wt% Mg at 600 °C. Although residual porosity is not uncommon in powder metallurgy parts and even in castings, its magnitude in the infiltrated part was worrisome. These pores can adversely affect the strength of material and parts and should be eliminated.

5.5 Elimination of Residual Porosity

One of the common methods to remove residual porosity is Hot Isostatic Pressing (HIP), where parts are subjected to high temperature and uniform high pressure in all directions simultaneously. Usually a pressure transmitting medium like gas or liquid is used to apply pressure uniformly from all directions. High-pressure differential between pores and outside environment causes the pores to collapse and removes all the residual porosity. The process results in full density and isotropic properties, especially in large

parts. However, for using hipping effectively, it is important that all the porosity in part is closed porosity only. Otherwise pressure transmitting medium, gas or liquid, will get into the pores and there would be no pressure differential to cause the collapse of the pores. So infiltrated parts were analyzed to check the nature of pores.

Measurements were done to determine percentage of closed porosity and open porosity (surface connected porosity) in the infiltrated parts. In the Archimedes test if instead of impregnating the sample with wax all the open pores were initially filled with water and then its wet weight (W_2) and submerged weight (W_3) were measured, the closed porosity, f_c (in %), and open porosity, f_o (in %), can be determined from the relations

$$f_c = \left(\frac{W_1 - W_3}{W_1} \frac{\rho_a}{\rho_w} - 1 \right) \rho_{app} \qquad [5.6]$$

$$f_o = 1 - f_c - \rho_{app} \qquad [5.7]$$

The apparent density of parts ρ_{app} can still be given by equation (5.5). Calculating porosity using these equations revealed that an infiltrated part had mostly open porosity. A typical infiltrated part had 3% open porosity and 6% closed porosity. This is not good, as hipping cannot be used for these parts to remove the residual porosity. So, parts were further analyzed to understand the causes of porosity.

There could be various mechanisms that caused porosity in the infiltrated part but the most plausible ones are non-wetting of certain regions of powder skeleton by the infiltrant and solidification shrinkage. It is possible that a region of the powder skeleton was having relatively thick oxide skin and it didn't break or magnesium couldn't reach certain regions of the powder part. As a result, infiltrant didn't wet these regions, causing residual porosity. Figure 5.8 shows the unmodified powder surface near pores, which implies non-wetting.

Attempts were made to remove these pores by adding additional magnesium in the powder preform itself. Elemental powders were first premixed in ball mill and then were lightly pressed in arbor press to make preforms. Fine magnesium powder (< 44 microns) was used for mixing with coarser aluminum powder (150-420 microns) to ensure uniform distribution of magnesium. 1-wt% of magnesium was added. This powder preform was

then infiltrated with an infiltrant containing 2-wt% Mg at 600 °C. The idea was that these premixed powders would ensure more uniform distribution of magnesium in the part and hence would help in breaking the oxides facilitating complete infiltration. These 1" parts infiltrated till the top but infiltrated part density was still 90% only. A more uniform distribution could be achieved if magnesium was present in the powder itself in pre-alloyed form. However, such powder was difficult to find. Moreover, that would reduce the melting point of powder preform, which could cause problem.

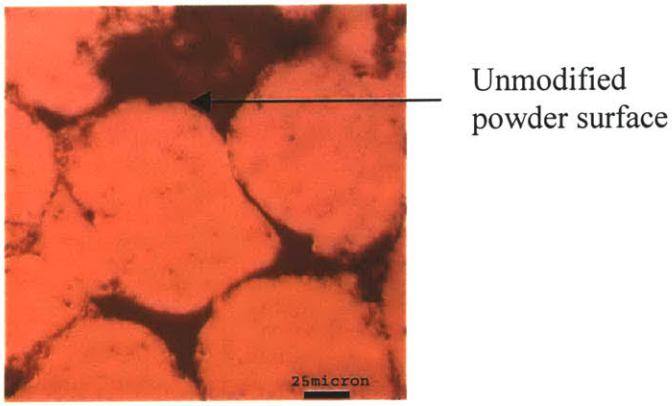

Figure 5.8 Pores due to non-wetting

Another mechanism that could contribute to residual porosity is solidification shrinkage. As discussed earlier, the infiltrated part have substantial amount of liquid at infiltration temperature. Therefore, when this liquid solidifies, it would shrink and this may lead to formation of shrinkage voids. Figure 5.9a shows the shrinkage voids in the infiltrated parts. The large pores like the ones shown in Figure 5.9b could be formed because of capillary induced flow of liquid formed inside the part to smaller pores when infiltrant supply is cut-off, leaving residual pores at the original site of the liquid [source 24].

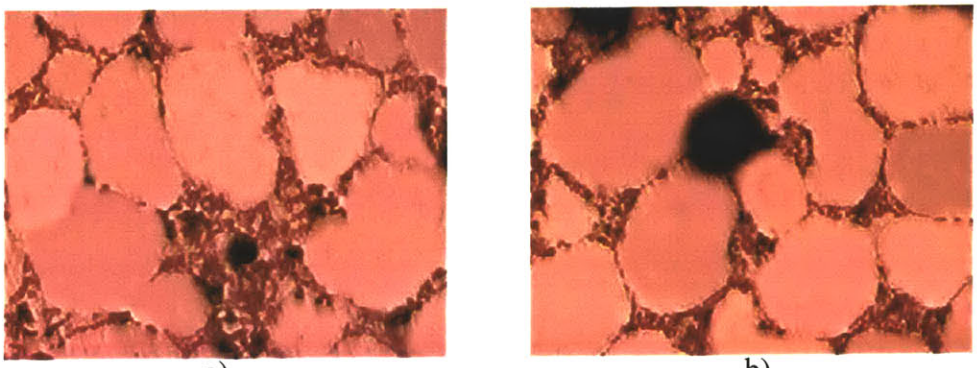

a) b)

Figure 5.9 Pores due to shrinkage and capillary induced flow

This shrinkage porosity could be minimized by maintaining liquid supply during solidification. Usually in gated infiltration, powder samples were dipped in the infiltrant at infiltration temperature and were removed from the melt before cooling. It was observed that during un-gated infiltration where parts were always in contact with infiltrant even during solidification, infiltrated part density was of the order of 95%. So gated infiltration experiments were conducted where part was dipped at infiltration temperature (620 ^{o}C) but it was left in contact with infiltrant even during cooling. The density of this infiltrated part was 96%. Figure 5.10 shows such an infiltrated part. The part had 2.8% closed porosity and 1.2 % open porosity.

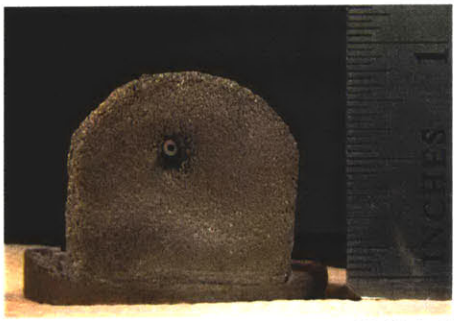

Figure 5.10 Infiltrated part (96% dense)

5.6 Mechanical Property Characterization

Mechanical testing was done on the infiltrated parts to characterize its mechanical properties like strength and hardness and a comparison was established with other similar common aluminum alloys. Hardness test is the most convenient way to determine mechanical properties of small sample parts, as is the case here. These hardness numbers can be converted to tensile strength values to get an estimate of the strength of the parts [23]. Therefore, Vickers microhardness tests were conducted on the infiltrated parts as per ASTM standards (Designation B 721-91). Especially for P/M materials, microhardness is useful and recommended for determination of the actual hardness of the metal matrix as it usually has some residual porosity.

Microhardness is measured by using a calibrated machine to force a diamond indenter of specific geometry, under a known test load, into the surface of the test material. The impression of the indenter is measured optically and these measurements are then used to

calculate a hardness number. For microhardness tests infiltrated specimens were first mounted in epoxy for convenience in surface preparation, edge retention, and testing. The surfaces of these samples were then prepared carefully as per the procedure mentioned in section 5.3 to obtain sound microhardness measurements. A microindentation hardness test was made in Vickers hardness tester using a test load of 25gf. A small load was used to avoid large indentations in aluminum samples so that indentations are confined in zones of interest only and doesn't go into pores. Table 5.1 shows the result of hardness test.

Table 5.1 Vickers Hardness Values (with 25gf load)

Infiltrated Sample	
Powder Region	31-35
Infiltrant Region	55-65
Pure Aluminum	28
5052 Al (2.5% Mg)	55
Al-Si alloy (3.5% Si)	43

Hardness measurements were done separately in powder region and infiltrated region as their hardness values will be very different because of presence of different phases and were repeated several times. For comparison, hardness values of some other similar common aluminum alloys were also determined.

Macrohardness test was also conducted on the infiltrated sample to get its average hardness value so that it can be compared more effectively with the standard alloys. Since aluminum is a very soft material, the recommended regular Rockwell scale for it, in the ASM Handbook is Rockwell H. Rockwell H hardness values of the infiltrated sample was determined using 1/8" ball indenter and 60 kgf major load. For comparison, macrohardness values of the same standard alloys were also measured and are listed in Table 5.2. The values shown are the average of five measurements. The measured Rockwell H values were converted to Brinell hardness numbers using the conversion table provided with the hardness tester. No Brinell hardness value for pure aluminum has been listed as its Rockwell H value was far beyond the minimum value listed in the table. The Brinell hardness value for Al-Si alloy (3.5% Si) was obtained by little extrapolation.

Table 5.2 Macrohardness Values

Sample	Rockwell H 1/8" ball, 60 kgf load	Brinell Hardness 500 kg load, 10 mm ball
Infiltrated Sample	88	55
Pure Aluminum	68	-
5052 Al (2.5% Mg)	97	66
Al-Si alloy (3.5% Si)	85	51

The listed Brinell hardness values for 5052 Al varies from 47 - 77 depending on the temper treatment. The Brinell hardness value for 5052-H34 Aluminum is 68 and its tensile strength and ultimate strength are 215 MPa and 260 MPa respectively. Similarly, the Brinell hardness value for 5052-H32 Aluminum is 60 and its tensile strength and ultimate strength are 195 MPa and 230 MPa respectively. The measurements show that the infiltrated part has higher hardness than pure aluminum and is comparable with other alloys.

Chapter 6. Conclusions and Future Work

6.1 Conclusions

This thesis work successfully demonstrates the feasibility of TLI in aluminum system. This should open up tremendous opportunities for freeform fabrication of aluminum metal parts. Parts of desired shape and complexity can be made directly from a CAD model by SFF processes like 3DP and will be densified near full density using transient liquid-phase infiltration without much dimensional changes.

Successful fabrication of fully dense aluminum metal parts by powder route is very difficult because of the presence of thick and dense natural oxides on the surface of aluminum powder which prevents wetting and solid state diffusion. The problem is even worse in the case of SFF processes where green part density is only at about 60% and there is no mechanical breakage of oxide layer, which generally occurs during mechanical compaction in conventional powder metallurgy processes. So, further processing of such green parts require more controlled furnace atmosphere which should be well cleaned to minimize oxygen content in the work zone. This will minimize the further oxidation of parts while processing and possibly reduce some of the existing oxides. This was achieved by using ultra high purity nitrogen gas and cleaning it even more by using aluminum gettering system. A pressed coarse aluminum powder disc placed upstream in the hot zone was used as a gettering agent as it removes oxygen by reacting with any oxygen present in the gas inflow before it enters the hot zone and hence provides clean atmosphere.

Use of gettering agent provides a very clean atmosphere for processing of aluminum. It significantly minimizes the growth of oxides at higher temperature during processing. However, it is doesn't reduce the oxides completely. Because of high reactivity of aluminum a strong, stable oxide film always encapsulates both infiltrant melt and powder skeleton. The oxide skin on the surface of infiltrant melt prevents infiltration as it inhibits liquid metal contact with the skeleton during gated infiltration. Therefore, it is necessary to get rid of oxide skin of the melt. This was realized by mechanically breaking the oxide

skin by pushing a ceramic foam filter from the top. The ceramic foam filter pushes the oxide skin to the bottom and clean liquid melt filters out from pores.

However, having clean melt in itself is not enough to facilitate infiltration in aluminum skeleton. The presence of dense, stable oxide layer on the surface aluminum powder prevents infiltration, as the liquid metal doesn't wet its oxide. Therefore, it is necessary to reduce or break the oxide on the skeleton to enable effective infiltration. A few different methods were tried to get around the problem. Coated aluminum powders, having a thin coating of relatively inert metal were used so that there is no oxide on the powder surface to start with. Experiments were done with silver, iron, copper, and nickel coated aluminum powder but no success was achieved in any case because of varied reasons like non-wetting or pre-mature coating failures due to diffusion. Finally, infiltration was achieved by using a wetting agent, magnesium, in the infiltrant. Trace addition of highly reactive element like magnesium in the melt enhances wetting by breaking the oxide layer as it preferentially reacts with oxygen and reduces the aluminum oxide. Once the oxide layer is broken, the melt diffuses through the cracks, lifts the oxide layer, and allows metal-metal contact to occur, facilitating infiltration.

Successful infiltration of 1" tall sample has been achieved with infiltrant containing 11-13 % Si and 2-4 % Mg. The height of the infiltrated sample was limited by the furnace size and not by the processing conditions and it can be easily scaled up for larger parts. The rate of infiltration is usually quite slow as compared with other infiltration because of gradual reactive rupture of the oxide skin. The microstructure of the infiltrated part is not a single-phase solid solution of the alloying elements in the base element. It contains aluminum powder particles with some diffused Si and Mg as primary phase and a two-phase field in the infiltrated area. The final part density of the infiltrated part varied from 90-96%, depending on processing conditions. The infiltrated part that was 96% dense had 2.8% closed porosity and 1.2% open porosity. This residual porosity can be removed by further processing like hipping or electroconsolidation, which is not uncommon in powder metallurgy. The infiltrated parts had strength comparable to similar commercial aluminum alloys.

6.2 Future Work

This work demonstrates successful implementation of TLI in aluminum system using model powder skeleton made by lightly pressing aluminum powder to 63-64% density. But it was never tried with real 3D printed part. Therefore, for complete demonstration of fabrication of aluminum metal parts by SFF processes, infiltration of real parts needs to be done. This might have its own issues because of complexities of shapes and residues left by binder burn-off.

Making aluminum metal parts by 3D printing in itself might involve some challenges because of binding and other issues and some research might be required in this area as well. Typically, PMMA is used as binder in aluminum metal parts.

Further research is required to explore and match the parts produced by TLI with more commercially available aluminum alloys, which are more common in typical applications. Finally, tensile testing of the real parts needs to done to establish a comparison with the parts produced by conventional processes.

Ag-Al

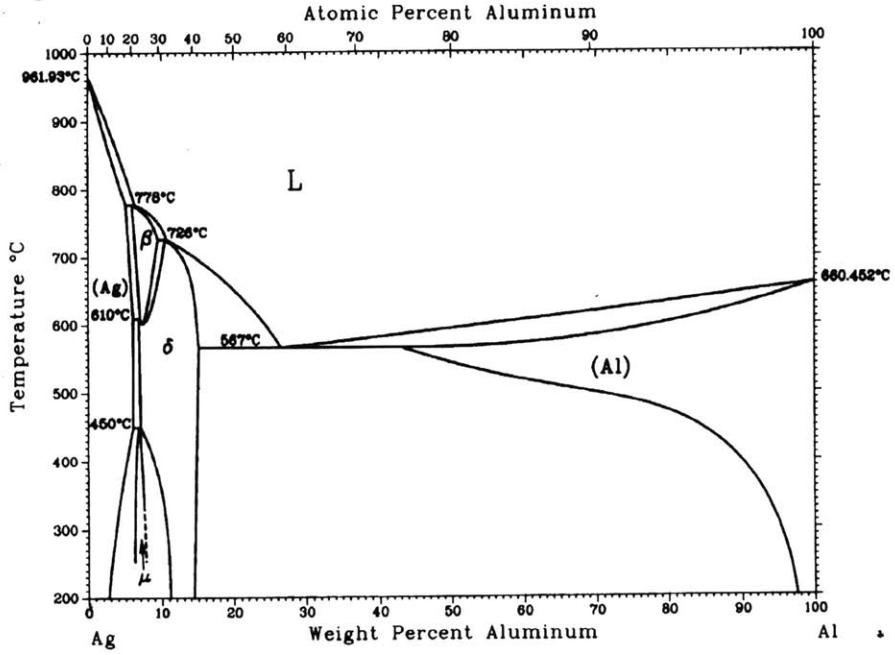
Atomic Percent Aluminum
Temperature °C
Weight Percent Aluminum
Ag
Al
961.93°C
778°C
726°C
610°C
567°C
450°C
660.452°C
L
β
(Ag)
δ
(Al)
ζ
μ

Al-Fe

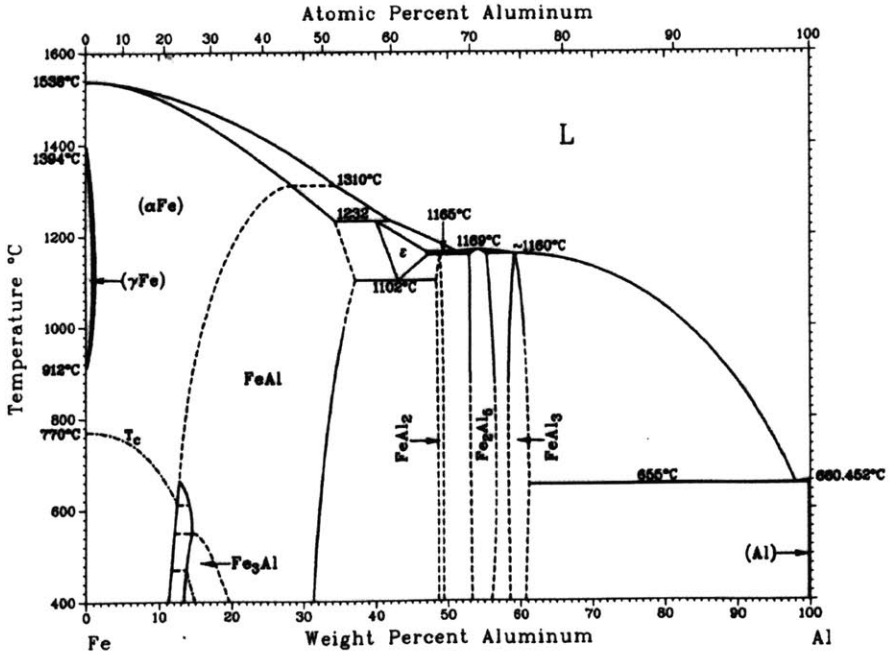
Atomic Percent Aluminum
Temperature °C
Weight Percent Aluminum
Fe
Al
1538°C
1394°C
912°C
770°C
1310°C
1232
1165°C
1169°C
~1160°C
1102°C
660.452°C
656°C
L
(αFe)
(γFe)
ε
FeAl
FeAl2
Fe2Al5
FeAl3
Tc
Fe3Al
(Al)

Al-Cu

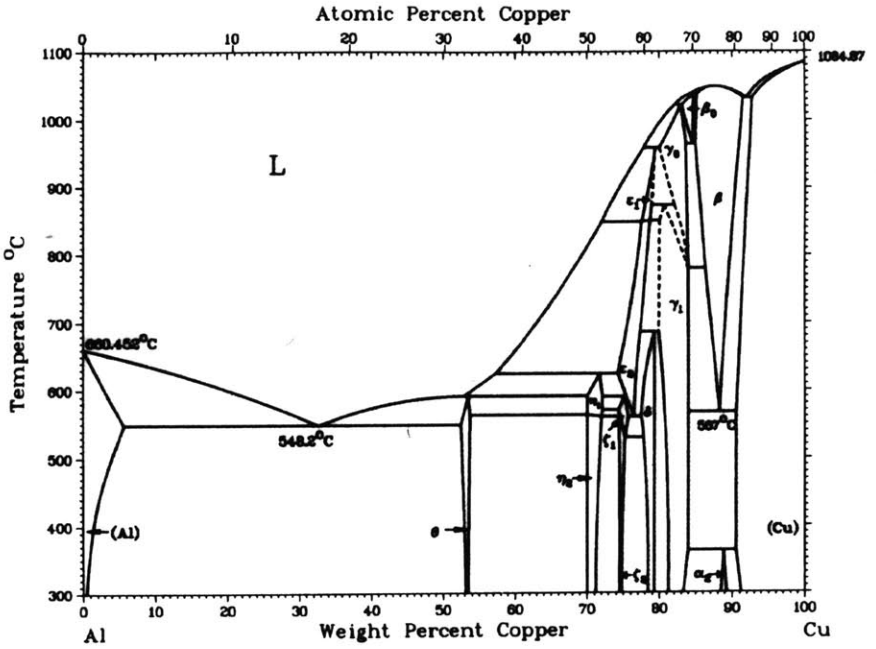
Atomic Percent Copper
Temperature °C
L
660.452°C
548.2°C
(Al)
(Cu)
Al
Weight Percent Copper
Cu

Al-Ni

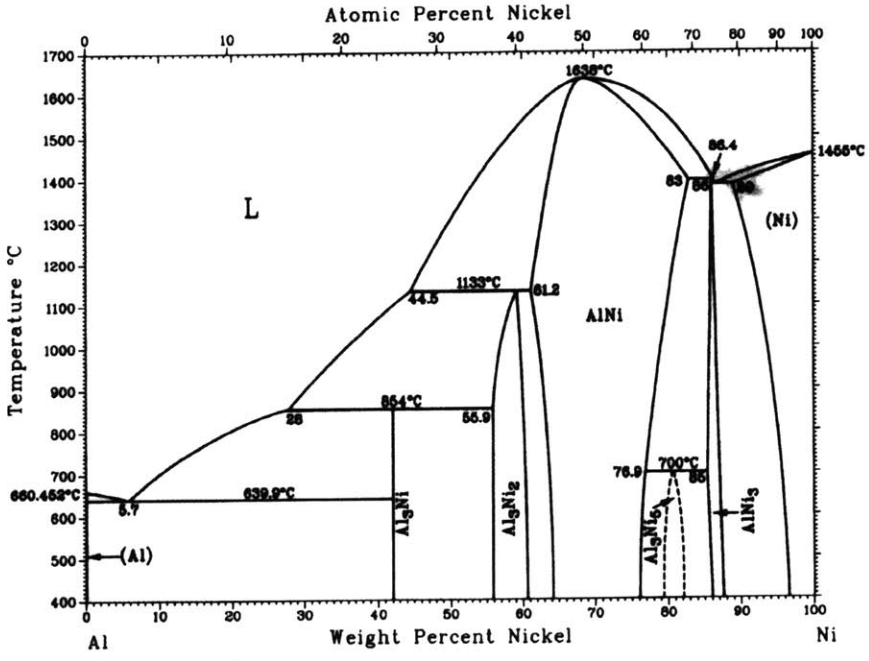
Atomic Percent Nickel
Temperature °C
L
1639°C
1455°C
(Ni)
1133°C
AlNi
854°C
660.452°C
639.9°C
(Al)
Al
Weight Percent Nickel
Ni

References

1. "ASM Specialty Handbook: Aluminum and Aluminum Alloys". Materials Park, Ohio: ASM International, 1993.
2. "Three Dimensional Printing", http://web.mit.edu/tdp/www/.
3. A. M. Lorenz, "*Transient Liquid-phase Infiltration of Powder Metal Skeleton*", PhD thesis, Massachusetts Institute of Technology, 2002.
4. Sachs et al, "*Novel Near-Net-Shape Tool-Less Method for Manufacturing of Cast Metal Matrix Composites: Three-Dimensional Printing (3DP) of Ceramic Preforms Combined with Investment Casting Technology*", SAE technical paper series, 2000-01-0675, SAE 2000 World Congress, Detroit, Michigan, March 6-9,2000.
5. T. B. Sercombe, G.B. Schaffer, P. Calvert, "*Freeform Fabrication of Functional Aluminum Prototypes using Powder Metallurgy*", J. of Materials Science (UK) 34, (17), pp 4245-4251, 1 Sept. 1999.
6. R. N. Lumley, T. B. Sercombe, and G.B. Schaffer, "*Surface Oxide and the Role of Magnesium during Sintering of Aluminum*", Metallurgical and Materials Transactions A, Volume 30A, pp 457-463, Feb 1999.
7. Y. Nakao, K. Sugaya, S. Seya and T. Sakuma, "*Process for Producing Aluminum Sintering*", United States Patent 5, 525,292, 1996.
8. John E. Gruzleski, and Bernard M. Closset, "*The Treatment of Liquid Aluminum-Silicon Alloys*", The American Foundrymen's Society Inc., Des Plaines, Illinois.
9. Tim Secombe, "Non-Conventional Sintered Aluminum Powder Alloys", B.E Thesis, University of Queensland, Australia, 1998.
10. I. A. Shibli and D. E. Davies, "*Effect of Oxidation on Sintering Characteristics of Al powder and effect on some minor metallic additions*", Powder Metallurgy, 1987, Vol. 30, No. 2, pp 97-101.

11. Z. A. Munir, "*Surface Oxides and Sintering of Metals*", Powder Metallurgy, 1981, No. 4, pp 177-179.

12. W. Kehl and H. F. Fischmeister, "*Liquid Phase Sintering of Al-Cu compacts*", Powder Metallurgy, 1980, No. 3, pp 113-119.

13. D. H. Kim, E. P. Yoon and J. S. Kim, "*Oxidation of an Aluminum-0.4 wt% Magnesium Alloy*", Journal of Materials Science Letters 15 (1996) 1429-1431.

14. "*Sintering of Aluminum parts: The State-of-the-Art*", Metal Powder Report, 1987, pp 354-358.

15. Daver et al., "*Aluminum P/M parts-Materials, Production and Properties*", Engineering Materials, Vol. 29-31 (1989) pp. 401-428.

16. J. H. Dudas and C. B. Thompson, "*Improved Sintering Procedures for Aluminum P/M parts*", Modern Developments in Powder Metallurgy, vol. 5, pp 19-36, 1971.

17. C. Lall, " *Fundamentals of High Temperature Sintering: Application to Stainless Steels and Soft Magnetic alloys*", The International Journal of Powder Metallurgy, Volume 27, No. 4, pp 315-329.

18. T. Magnusson and L. Arnberg, "*Density and Solidification Shrinkage of Hypoeutectic Aluminum-Silicon Alloys*", Metallurgical and Materials Transactions A, Volume 32A, 2001, pp 2605-2613.

19. D.C. Dunand, J. L. Sommer and A. Mortensen, "Synthesis of Bulk and Reinforced Nickel Aluminides by Reactive Infiltration", Metallurgical Transactions A, Volume 24A, October 1993, pp 2161- 2170.

20. "*Standard Test Methods for Microhardness and Case Depth of Powder Metallurgy Parts*", ASTM standard, Designation: B 721- 91 (Reapproved 1999), ASTM international.

21. S. –J. L. Kang, W. A. Kaysser, G. Petzow, and D. N. Yoon, "*Elimination of Pores during Liquid Phase Sintering of Mo-Ni*", Powder Metallurgy, 1984, Vol. 27, No.2, 97-100.

22. Coating of powder by Fluidized Bed Chemical Vapor Deposition processing technology, http://www.powdermetinc.com/technology.htm.

23. Michael F Ashby and David R H Jones, "*Engineering Materials 1: An Introduction to Their Properties and Applications*", Second Edition, Butterworth-Heinemann, pp 113-114.

24. S. J. L. Kang, W. A. Kassyer, G. Petzow, and D. N. Yoon, "*Elimination of Pores during Liquid Phase Sintering of Mo-Ni*", Powder Metallurgy, vol. 27, pp 97-100, 1984.

25. S. W. Ip, M. Kucharski and J. M. Toguri, "*Wetting Behavior Aluminum and Aluminum-Alloys on Al_2O_3 and CaO*", J. Mater. Science Letter, 1993, vol.12, pp1699-1702.

26. Y. Liu, Z. He, S. Yu, G. Dong, and Q. Li: J. Mater. Science Letter, 1992, 11, pp 896-98.

27. Munir Z. A, "*Analytical Treatment of the Role of Surface Oxide Layers in the Sintering of Metals*", J. Mater. Science, 1979, vol. 14, pp 2733-40.

28. Kovacs I, Lendvai J, Ungar T, "*Investigation of Mg Loss During Heat-Treatments in an Al-Mg-Si Alloy*", Materials Science And Engineering, 21 (2): 169-175 1975.

29. C. G. Levi, G. J. Abbaschian, and R. Mehrabian, "*Interface Interactions During Fabrication of Aluminum Alloy-Alumina Fiber Composites*", Metallurgical Transactions A, vol. 9A, pp 697-711, 1978.

30. "*Diffusion in Solid Metals and Alloys*", Volume III/26, online edition, http://link.springer.de/link/service/series/0284/tocs/003/t0030000026.htm